PRELIMINARY INVESTIGATION OF A POSSIBLE DOSE RATE EFFECT ON SURVIVAL OF CELLS IRRADIATED WITH LOW ENERGY PROTONS

L.P.G. Robinson

UNIVERSITY OF CAPE TOWN

DEPARTMENT OF PHYSICS

PRELIMINARY INVESTIGATION OF A POSSIBLE DOSE RATE EFFECT ON SURVIVAL OF CELLS IRRADIATED WITH LOW ENERGY PROTONS

L.P.G. Robinson

Thesis submitted in fulfilment of the
requirements for the degree of

MASTER OF SCIENCE

in the Faculty of Science
January 1989

ABSTRACT

Apparatus has been developed for the irradiation of V79-379A Chinese hamster lung fibroblast cells with 3.6 MeV protons from the Van de Graaff accelerator at the National Accelerator Centre in Faure. The original intention of this work was to investigate and measure a possible dose rate effect on the survival of V79 cells, in the dose range from zero to 25 Gy, at dose rates of about 3 Gy/s and 300 Gy/s. The survival curves initially obtained were anomalous in that they showed abnormally high levels of survival and a tendency to remain at a constant survival level for doses above 10 Gy. Systematic attempts to correct this observed anomaly involved the following; apparatus improvements were made, a means of measuring the beam profile was devised, the current measuring device and the dosimetry were improved and a possible dose rate effect on intracellular oxygen was investigated. After these improvements, the anomalous effect was much reduced, but not entirely eliminated.

The final results showed no significant difference between the survival of cells irradiated at dose rates of about 3 Gy/s and 300 Gy/s; qualitative differences were however noticeable. After correction for the effect of a non-uniform beam profile, the survival curves were significantly different to published work. This difference suggested a possible dose rate effect between dose rates of about 0.1 Gy/s and dose rates above 3 Gy/s.

ACKNOWLEDGEMENTS

I wish to express my appreciation and gratitude to:

Professor R.D. Cherry (UCT), Dr. D.T.L. Jones (NAC) and Dr. L. Bohm (US), my supervisors, for their help and guidance during the project and for their advice on the compilation of this thesis;

The staff of the Radiobiology Laboratory at the Stellenbosch Medical Faculty for their help with the biological aspects of this work as well as their friendly encouragement;

The scientific and technical staff of the National Accelerator Centre's Van de Graaff Group for their advice and help with the experimental work, and for the construction of the required apparatus;

The many friends and family who painstakingly helped with the experimental work and with the typing and checking of the manuscript;

My parents for their lengthy support and encouragement with my studies.

TABLE OF CONTENTS

1 CHAPTER ONE: OVERVIEW

1.1 INTRODUCTION

In 1946 Wilson published a paper on the physical properties of heavy charged particles and their potential use in radiotherapy (Wilson, 1946). At that time, the 184-inch cyclotron at Berkeley was under construction. This cyclotron was capable of producing protons, deuterons and alpha particles with intensities and ranges sufficient for radiotherapy. When the present work commenced, a cyclotron capable of accelerating protons to an energy of 200 MeV was under construction at Faure in South Africa. This multidisciplinary facility was designed to be used for basic nuclear research, radionuclide production and radiotherapy with neutron and proton beams. Protons with an energy of 200 MeV have a range of about 26 cm in tissue (Janni, 1982) and are therefore suitable for treating most sites within the body.

Protons penetrate tissue in an almost straight line. As the proton proceeds through the tissue, tissue atoms are ionised at the expense of the proton energy. The dose delivered to the tissue (energy deposited per unit mass) is proportional to the specific ionisation which varies almost inversely with the energy of the proton. Thus the specific ionisation is much less where the proton enters the tissue at high energy than it is in the last portion of its path. This property was noted by Bragg and Kleeman (1904). The energy loss curve (Bragg ionisation curve) therefore exhibits a relatively flat entrance

region followed by a sharp dose peak (the Bragg peak) at the end of the range. Figure 1.1 shows the Bragg ionisation curve for protons with an energy of 140 MeV. Note that the dose increases by a factor of three in the last centimetre of the proton's range and immediately thereafter is reduced to zero.

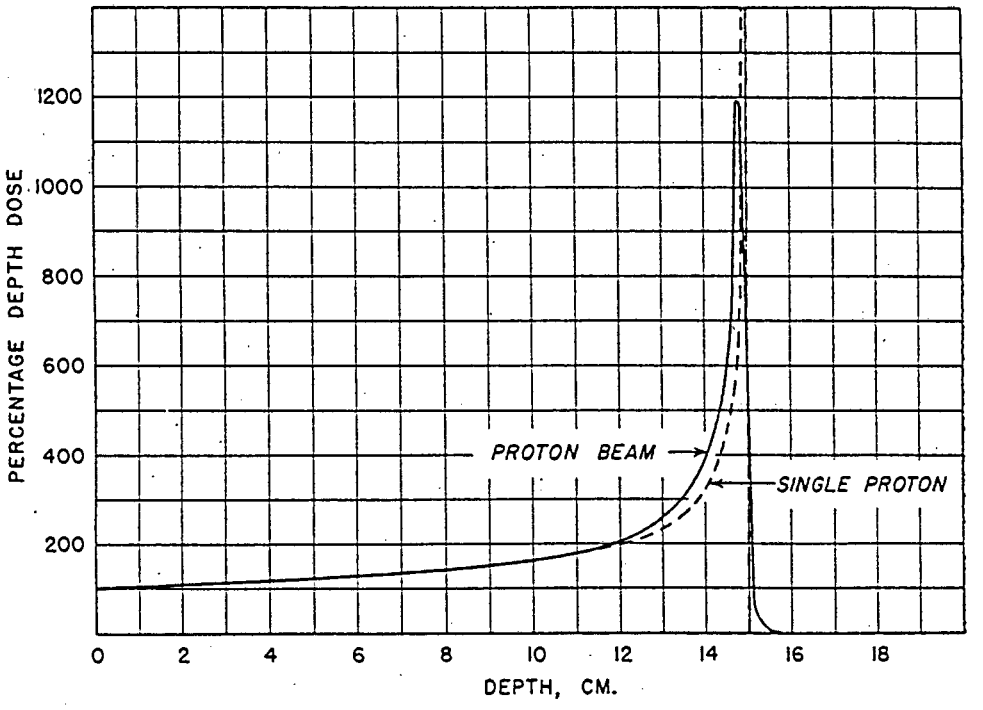

Figure 1.1 The dotted curve shows the relative dose due to a single 140 MeV proton. The full curve shows qualitatively the depth dose curve for a beam of 140 MeV protons in tissue (taken from Wilson, 1946).

The phenomenon of the Bragg peak, coupled with the definite range of protons (dependent on the initial energy), beyond which the dose is zero, together offer the potential for localising the dose in the tumour and minimising the dose to the surrounding normal tissue, thus making protons very desirable for radiotherapy.

The production of large fields for proton radiotherapy can be achieved either by coulomb scattering of the primary beam until the required field size and beam uniformity is obtained (Koehler et al., 1977), or by scanning a pencil beam horizontally and vertically with electromagnets (Larsson, 1961; Larsson and Sarby, 1975). This second option was under discussion, for the facility at Faure, when the present work was proposed.

When attempting to utilise the localisability advantages of proton beams on deep seated tumours, organ movement may cause some of the advantages to be lost. This situation prompted the suggestion that the irradiation be done very quickly thus minimising the extent of organ movement during irradiation. The problem of geographically missing the tumour is then reduced to a matter of accurate beam delivery.

If the time scale chosen for irradiation is one second rather than the conventional few minutes and if we assume a beam area of 16 mm^2 and a radiation field of 25 cm^2 and assume that the dose required per treatment is 5 Gy, then the instantaneous dose rate at each 16 mm^2 point would have to be nearly 800 Gy/s. Such high dose rates have never been used in therapy. The effects of such high dose rate irradiation have not been widely studied. The effect of cell inactivation (cell survival as measured by the cell's colony-forming ability after irradiation) needs to be investigated.

The aim of this work was twofold, with the emphasis on (1) below:

(1) To develop apparatus and experimental techniques for performing low energy proton irradiation of mammalian cells on a Van de Graaff accelerator. This experience would form the foundation for later work on the 200 MeV proton beam facility.

(2) To use the experience gained and the facilities developed to perform a preliminary investigation of a possible dose rate effect on survival of cells irradiated at dose rates of about 3 Gy/s and 300 Gy/s.

1.2 BACKGROUND THEORY

1.2.1 THE INTERACTION OF HEAVY CHARGED PARTICLES WITH MATTER

Heavy charged particles undergo electromagnetic and nuclear interactions with matter. In the case of protons with energy less than 10 MeV, electromagnetic interactions are the important interactions, (Fitzgerald et al., 1967) and therefore only these will be dealt with here.

Three types of electromagnetic interactions of heavy charged particles with matter can be identified (Fitzgerald et al., 1967):

(1) If the distance of closest approach to an atom is large compared with atomic dimensions, then the charged particle reacts with the atom as a whole. The result is excitation or ionisation of the atom and slight deflection of the incident charged particle. If ionisation occurs then the energy of the freed electron will be quite small.

(2) If the distance of closest approach to an atom is of the order of atomic dimensions, then the interaction of the charged particle is with an individual electron in the atom. The electron is usually freed from the atom and escapes with considerable energy. These escaping electrons are called delta rays. The trajectory of the incident particle will not be significantly altered by

such an interaction.

(3) If the distance of closest approach to an atom is significantly small compared with atomic dimensions, then the deflection in the trajectory of the incident particle caused by the electric field of the nucleus becomes significant. This process can often be accompanied by the emission of photon radiation called bremsstrahlung, and is then known as inelastic nuclear scattering, while the absence of bremsstrahlung indicates that kinetic energy has been conserved and the process is then known as elastic nuclear scattering.

The most probable types of encounters, particularly for protons with an energy less than 10 MeV, are the distant ones described in (1) and (2) above (Fitzgerald et al., 1967). The transfer of energy from the incident particle to the medium therefore takes place through the ionisation and excitation of the atoms of the medium through which it passes.

An important parameter is the specific energy loss as this has a bearing on the biological effects produced. The specific energy loss or linear stopping power, S, is expressed as:

$$S = -\frac{dT}{dx} \qquad (1.1)$$

Where T is the kinetic energy of the particle and x is the pathlength over which the energy is dissipated.

This is often called the "linear energy transfer" (LET) by radiobiologists. Strictly speaking, LET and stopping power do not necessarily convey the same information. LET is used to describe the energy deposited in the target volume by the incident radiation. Secondary electrons or photons which are emitted by the interaction of the primary radiation often have a high enough energy to escape from the immediate vicinity of the primary interaction. In this case, the secondary energy deposited outside the target volume will not be included in the evaluation of LET. On the other hand, stopping power is used to describe the energy lost by the incident radiation in an interaction. The final position at which that energy is deposited is unimportant and hence LET can be lower than stopping power. Fortunately, when the incident radiation is in the form of protons, the secondary radiation has a low energy and is usually absorbed within a short distance of its creation. Brustad (1962) gives an expression for the maximum kinetic energy, T, that can be transferred to an electron by a heavy charged particle:

$$T = 2\,mc^2 \left(\frac{\beta^2}{1-\beta^2}\right) \qquad (1.2)$$

where m is the rest mass of the electron and β is the velocity of the heavy ion relative to the speed of light, c.

For example, for protons with a kinetic energy of 4 MeV, the maximum electron kinetic energy is about 8 keV. These

electrons have a range in tissue of only 2.5 μm (ICRU, 1984) and will hence be absorbed very close to their site of creation. For this reason, LET is considered to be essentially the same as stopping power for low energy protons (Wilson, 1946; Kellerer and Chmelevsky, 1975).

The concept of stopping power is related to the concept of the range of a charged particle. The range, R, may be expressed as:

$$R = \int_0^R dx = \int_0^{T_0} \frac{dT}{S} \qquad (1.3)$$

where T_0 is the initial kinetic energy of the charged particle and x is a pathlength.

Since the processes of energy loss by charged particles in matter are statistical in nature, the range for various particles of the same type with the same initial energy will have a statistical spread about a mean value. This is known as range straggling. Range straggling for protons and heavier ions is only a small fraction of the particle's range and can often be ignored in practice. For example, the range straggling of a proton with kinetic energy of 4 MeV is less than two per cent of the range (Janni, 1982).

The theory of ionisation and specific energy loss by heavy charged particles is based on work done by Bethe (1930) amongst others. The Bethe formula for the mean rate of ionisation loss

of a charged particle is given by equation 1.4 (Perkins, 1982).

$$S = \frac{4\pi N_0 z^2 e^4}{mv^2} \frac{Z}{A} \left[\ell n \left(\frac{2mv^2}{I(1-\beta^2)} \right) - \beta^2 \right] \qquad (1.4)$$

where: z = the atomic number of the incident ion.

e = the elementary electronic charge.

v = the velocity of the incident ion.

Z = the atomic number of the absorbing medium.

A = the mass number of the absorbing medium.

N_0 = Avogadro's number.

m = the electron rest mass.

I = the average ionisation potential of atoms of the medium.

β = the velocity of the incident ion relative to the velocity of light.

Theoretically, the range of a charged particle could be calculated by integrating equation 1.4 from the initial kinetic energy down to zero energy. One of the assumptions on which the Bethe equation is based is, however, that the particle's velocity is greater than the velocity of the atomic electrons of the absorbing medium. Integration of equation 1.4 thus introduces an error in the range from the low energy region of the particle's path. The range is therefore best determined experimentally or from empirical formulae.

The ranges of protons (in various media) used in this work are

obtained from the work of Janni (1982). He used empirical and theoretical formulae which he has developed into a model which gives good agreement with experimentally measured values.

1.2.2 DOSE-EFFECT MODELS

Little can be understood about the biological effect of radiation unless it is related to the "dose" of radiation which is causing the effect. The term "dose" (as used in radiotherapy) refers to the "absorbed dose", which is equal to the energy absorbed by the tissue per unit mass. The S.I. unit for radiation dose is the gray (Gy), which is defined as one joule of energy absorbed per kilogram of tissue. The older unit, the rad is still commonly used and is defined as 100 erg of energy absorbed per gram of tissue. One rad is equivalent to 0.01 Gy or 10 mGy.

The concepts of "hits" and "targets" are central to radiobiology and to the development of formal models relating to cell inactivation. The concept of a "hit" is related to the physics of the interaction of radiation with matter. The "target" zone is often thought to be the DNA molecule, but can in general be considered to be any sensitive site, within a cell or organism, which if "hit" by radiation will result in some measurable biological effect. The most important effect is that of cell inactivation which can be expressed by intermitotic death (large radiation doses, tens of gray) and by reproductive failure (small doses, less than 10 Gy) (Coggle,

1983). A cell which has been inactivated by radiation may still have a normal morphology, physiology and biochemistry, but when the cell enters the metaphase stage of the cell cycle and starts dividing, the damage to the DNA may manifest itself and will be expressed in the daughter cells. Eventually, the inherited genetic deficiencies will result in the descendent cells being unable to continue dividing.

Cell survival is usually measured by the cell's ability to form a colony of between 40 and 60 cells. This corresponds to about five cell divisions and is generally considered a sufficient test for reproductive integrity.

Cell inactivation by radiation requires three related steps:

(1) The cell's absorption of energy from the radiation.

(2) The production of molecular lesions, which are radiation induced chemical reactions, in sensitive sites.

(3) The biological expression of these lesions.

When only a single "hit" is required to inactivate a target and when the inactivation of any one target results in reproductive failure, the dose-response curve is governed by the fact that energy is deposited at random, in accordance with Poisson statistics. This leads to the mathematical form for the surviving fraction f as:

$$f = e^{-\frac{D}{D_0}} \qquad (1.5)$$

or

$$f = e^{-CD}$$

where D_∞ is called the inactivation dose, c ($=1/D_\infty$) is called the inactivation constant and corresponds to the slope of the linear portion of the survival curve (see figure 1.2), and D is the absorbed dose (Alper, 1979).

Many bacteriological studies result in an exponential survival curve of this form. For biologically more complex cells, however, the survival curves often have an initial shoulder in the low dose region, particularly when irradiated with low LET (less than about 10 keV/μm) radiation, such as high energy protons, x-rays and gamma-rays. This shoulder represents the cells ability to repair some radiation damage (called sublethal damage). Typical cell survival curves are shown in Figure 1.2. These curves are characterised by two parameters: the inactivation dose, D_∞, the dose required to reduce the surviving fraction by 63%, and the extrapolation number, n, the value at which the linear portion of the survival curve, extrapolated to zero dose, intercepts the logarithmic axis (Alper et al., 1960).

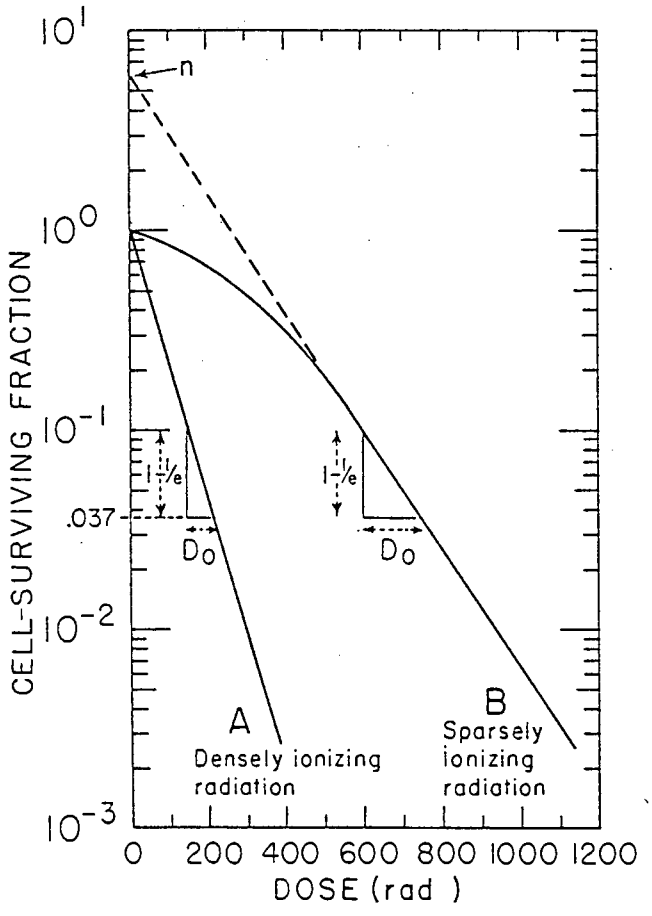

Figure 1.2 Typical survival curves for mammalian cells exposed to radiation of low (B) and high (A) LET. The fraction of surviving cells is plotted on a logarithmic scale against dose on a linear scale (Alper et al. 1960). (Taken from Hall, 1978) (1 rad = 0.01 Gy).

1.2.2.1 THE MULTI-TARGET SINGLE-HIT MODEL

The frequent occurrence of shouldered survival curves gave rise to the multi-target, single-hit concept (Elkind and Whitmore, 1967). Suppose that a cell contains n identical targets and that the cell can proliferate if only one target remains undisturbed. Suppose also that the inactivation constant for each target is c. After a dose D, the probability of any target surviving is exp(-cD). The probability that all n targets will have been inactivated is $(1-\exp(-cD))^n$, which is

also the probability that the cell will have been inactivated. Therefore, the probability of survival is $1-(1-\exp(-cD))^n$. The surviving fraction f is then given by:

$$f = 1 - \left(1-e^{-CD}\right)^n \qquad (1.6)$$

at large doses D, this reduces to:

$$f = ne^{-CD}$$

Survival curves are usually plotted on a semi-logarithmic set of axes, with a logarithmic ordinate and a linear abscissa as in figure 1.2. Therefore on a logarithmic scale, the surviving fraction, f, becomes:

$$\ln f = \ell n\, n - CD \qquad (1.7)$$

and hence, the survivial curve becomes a straight line at high doses (see figure 1.2).

According to equation 1.6, the survival curve should have a zero slope at zero dose. This, however, is seldom observed. For example, a non-zero slope at zero dose would be expected if the cell population was inhomogeneous with respect to the number of targets per cell.

Further refinements of the models that give rise to equation 1.6 yield a more general form:

$$f = e^{-C_1 D}\left[1 - \left(1-e^{-C_2 D}\right)^n\right] \qquad (1.8)$$

where the term $\exp(-c_1 D)$ has been included to account for the frequently observed non-zero slope at zero dose.

The above equations 1.6 and 1.8 were utilised by Puck and Marcus (1956) who constructed the first mammalian cell survival curve using tissue culture techniques.

1.2.2.2 THE MOLECULAR MODEL FOR CELL SURVIVAL

Chadwick and Leenhouts (1973 a,b) considered DNA to be the crucial radiation target and devised a mathematical model which relates the number of DNA double strand breaks to cell survival. The average number, N, of DNA double strand breaks per cell induced by a radiation dose D is given by:

$$N = aD + bD^2 \qquad (1.9)$$

where a = single event action and b = double event action.

Although applying microdosimetric considerations, Kellerer and Rossi (1972) postulated the same relationship between the average number of DNA double strand breaks and the absorbed dose.

If p is the probability that an unrepaired DNA double strand

break leads to cell reproductive death, and if $N=aD+bD^2$ is the average number of DNA double strand breaks per cell which is induced in a uniform population of synchronised single cells by a radiation dose D, and if f_p is the fraction of DNA double strand breaks that remain unrepaired by the cell, then f_pN is the average number of unrepaired double strand breaks and pf_pN is the average number of "lethal events" per cell. From the Poisson distribution of lethal events per cell, cell survival, f, is given by (Chadwick and Leenhouts, 1981):

$$f = e^{-P(aD+bD^2)} \qquad (1.10)$$

For simplicity, radiobiologists often use:

$$f = e^{-(\alpha D+\beta D^2)} \qquad (1.11)$$

where α now replaces pa and β replaces pb.

In logarithmic form, this reduces to:

$$\ell n\ f = -(\alpha D+\beta D^2) \qquad (1.12)$$

and hence cell survival, according to this model, follows a parabola when plotted on a semi-logarithmic set of axes.

In the above summary, only the most common models in radiobiology have been presented. Other more sophisticated models which include a term to account for repair of sublethal

damage have been excluded since they are not relevant to this work.

1.2.3 COMPARATIVE PARAMETERS

Two parameters fequently used in radiobiology, irrespective of the survival model chosen, are RBE and OER.

1.2.3.1 RELATIVE BIOLOGICAL EFFECTIVENESS (RBE)

Equal doses of different types of radiation do not necessarily produce the same biological effect. A standard radiation (often 250 kV x-rays or cobalt-60 gamma radiation) is chosen as the reference to compare different radiation types. The formal definition of RBE is as follows:

The RBE of some test radiation (r) compared with a reference radiation (ref) is defined by the ratio D_{r-ref}/D_r, where D_{r-ref} and D_r are, respectively, the doses of reference radiation and the test radiation required to produce equal biological effect (Hall, 1978). The biological effect is usually a specific survival level, for example, 1% or 37%, but in general, any suitable level may be used.

For example, if the radiation type which gave rise to curve B in figure 1.2 is chosen as the reference radiation, then the RBE, at a survival level of 0.01, of the radiation type which

gave rise to curve A, is approximately 3.13 (9.4 Gy divided by 3 Gy).

1.2.3.2 OXYGEN ENHANCEMENT RATIO (OER)

Typical survival curves for mammalian cells exposed to x-rays under aerated and hypoxic conditions are shown in figure 1.3. Although the general shape of the survival curves is the same, the dose required to achieve a surviving fraction of 0.01 for the hypoxic cells is three times the dose required for the aerated cells. This ratio is called the oxygen enhancement ratio (OER) and is calculated in the same way as the RBE (with the hypoxic survival curve acting as the reference curve). For a given type of radiation, the OER is usually independent of dose or survival level. For low LET radiation, such as high energy protons, x-rays or gamma-rays, the OER typically has a value between 2.5 and 3.0 (Hall, 1978)

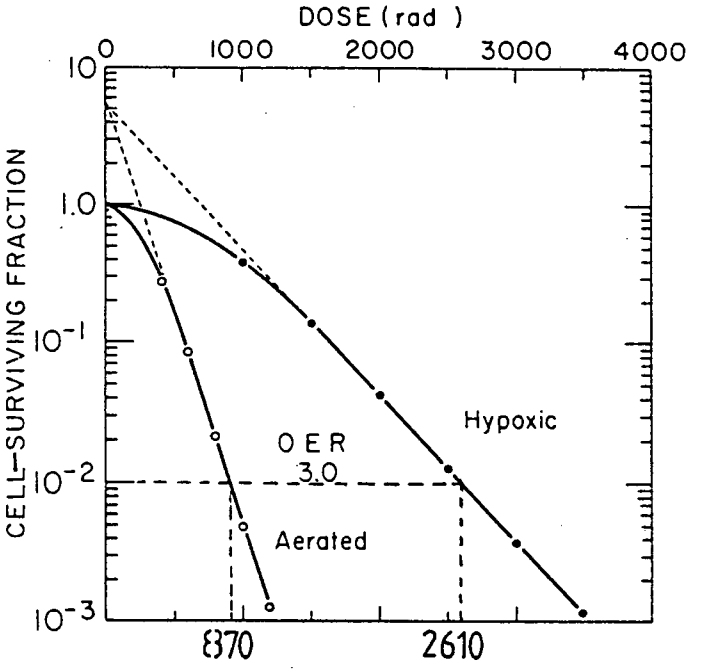

Figure 1.3 Survival curves for cultured mammalian cells exposed to x-rays under aerated and hypoxic conditions (From Hall, 1978) (1 rad = 0.01 Gy).

For very high LET radiation (above 160 keV/μm), such as low energy heavy ions, the OER approaches unity (Raju, 1980). For fast neutron radiation, considered high LET (above 100 keV/μm), the OER is approximately 1.6 for a large range of biological systems and is independent of neutron energy (Hall, 1978).

When one considers that the centres of tumours are often less well oxygenated than normal tissue, because of poor blood supply, and hence less sensitive to conventional low LET radiation, a radiation type with a low OER is therefore desirable for treating these tumours. This was one of the major reasons for the introduction of high energy neutrons in radiotherapy.

1.3 EXPERIENCE WITH PROTON BEAMS

The potential use of protons in radiotherapy was first proposed by Wilson (1946). A few years later, these proposals were realised when the work of Tobias et al. (1954) at Berkeley led to the use of protons and other heavy ions in treating diseases of the pituitary gland. Since that time, considerable experimental and clinical work has been conducted and this has led to the use of protons and other heavy ions in treating a number of other sites. This work has been extensively reviewed by Raju (1980). The major clinical advantage offered by protons is the superior dose distribution which is possible with these particles (Hall, 1981; Suit et al., 1977; Suit et al., 1975; Archambeau et al., 1974; Koehler et al., 1972) which allows the dose delivered to be better confined to the treatment volume than with x-rays and gamma radiation. Hall (1981) has compared the advantages of heavy charged particles with other types of radiation. His findings are best summarised in figure 1.4, in which he compares the dose distribution advantage with the high LET advantage for a number of radiation types. The high LET advantage refers to the increased RBE and decreased OER which is observed with high LET radiation.

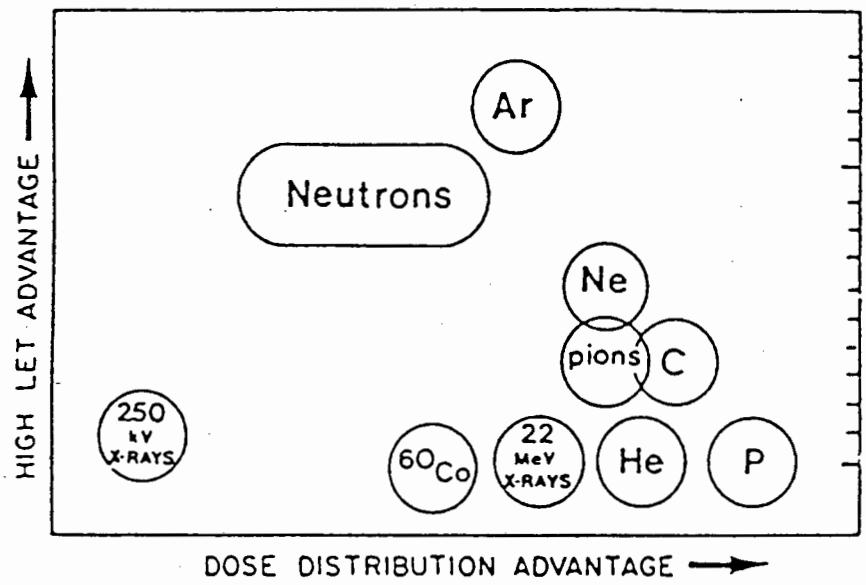

Figure 1.4 The particles compared. On one axis is plotted the advantage of dose distribution and on the other the benefits of high LET. Clearly, protons provide the best dose distributions. (Taken from Hall, 1981).

In spite of the favourable properties of protons and the favourable clinical experience with their use, protons are not widely used in radiotherapy largely because costly accelerators are required for their production. Goitein et al. (1985) have reviewed the current status of low LET charged particle radiation therapy (which includes protons and helium ions). They note the problems associated with exploiting the favourable depth dose characteristics of protons. Specifically, the penetration of protons is sensitively dependent on the composition of the material traversed. The planning of treatment therefore requires the determination of tissue densities throughout the volume of interest and the development of techniques to include the effect of tissue

heterodensities on dose. They note that computed tomography (CT), at an appropriate resolution, is available to map these heterodensities and that while the exact computation of dose in the presence of inhomogeneities is difficult, simplified approximations have been shown to be satisfactory. Goitein et al. (1985) also note that the technical problems associated with accurate and reliable beam delivery have been largely overcome, while problems with the greater accuracy required in patient positioning have been adequately solved by using individualised moulds, casts and bite blocks.

Goitein et al. (1985) note some of the clinical successes in proton beam therapy, such as the treatment of arteriovenous malformations, pituitary disorders, choroidal melanomas, chordomas and chondrosarcomas close to sensitive central nervous system structures and paraspinal soft tissue sarcomas. They suggest an expansion of low LET charged particle therapy facilities and advocate exploring the application of low LET particle radiation to more treatment sites.

Much work has been published on the determination of the RBE of high energy protons using a variety of endpoints (Urano et al., 1984; Urano et al., 1980; Hall et al., 1978; Suit et al., 1977; Tepper et al., 1977). A fairly wide range of values have been reported, both for the RBE of protons relative to 250 kV X-rays or cobalt-60 gamma rays and for the RBE in the Bragg peak relative to the plateau region of the proton beam ionisation curve (Raju, 1980; Robertson et al., 1975; Archambeau et al.,

1974). Robertson et al. (1975), using the 160 MeV proton beam from the Harvard cyclotron showed that the RBE of those protons relative to cobalt-60 gamma rays was 1.00 ± 0.01 in the plateau region and approximately 1.4 at the distal portion of the Bragg peak. They note that the differences in the RBE values reported by other authors could be a function of the biological endpoints used. They conclude that since the RBE of protons from the modulated beam at Harvard is not significantly different from unity except at the distal portion of the Bragg peak, cobalt-60 gamma ray treatment techniques could be used with protons.

A limited amount of work on the biological effects of low energy protons has been published, Perris et al. (1986), Bettega et al. (1979) and Wainson et al. (1972) all report an increase in RBE for protons with energy below 8 MeV. Perris et al. (1986) report an RBE (relative to cobalt-60 gamma radiation) of 1.7 ± 0.1 and 2.8 ± 0.2 for 7.4 MeV and 3.0 MeV protons respectively, using V79 cells. Bettega et al. (1979) report an RBE (relative to cobalt-60 gamma radiation) of 1.0 ± 0.1, 1.4 ± 0.2 and 1.5 ± 0.2 for 31 MeV, 12 MeV and 8 MeV protons respectively, using the EUE cell line. Wainson et al. (1972), using HeLa cells and B-11-d-ii-FAF-28 cells, have shown that the RBE of 8 MeV protons relative to both 90 MeV and 28 MeV protons is 1.44 ± 0.08. These authors all relate the increase in RBE to the increase in LET as the proton energy decreases. This is confirmed by Bird et al. (1980) who have shown, using particles of different LET, that RBE increases

with increasing LET. Perris et al. (1986) point out that LET may not be the ideal parameter to correlate with RBE and suggest that specific primary ionisation might be more appropriate. They also note that radiobiological data from low energy proton beams are scarce and that there is therefore a need for more work with low energy beams.

1.4 DOSE RATE EFFECTS

Although the present work largely involves the development of experimental techniques associated with the irradiation of biological systems with low energy proton beams, it is appropriate to review the current understanding regarding dose rate effects on cell survival, as this was the motivation for developing the present techniques.

Dose rate studies, using photons, have been carried out over a wide range of dose rates and have been reviewed extensively by Hall (1972). The range of dose rates that has been investigated is shown in figure 1.5. The most significant dose rate effect is observed in the dose rate range from 0.1 Gy/hour to 10 Gy/min. (Fu et al., 1975; Mitchell et al., 1979a,c; Bedford and Mitchell, 1973; Hall and Bedford, 1964). This is shown in figure 1.6 and figure 1.7 for two specific cell lines. The trend shown in these figures is typical and illustrative of the dose rate effect in this dose rate range and is thought to be due to the repair of sublethal damage within the cells.

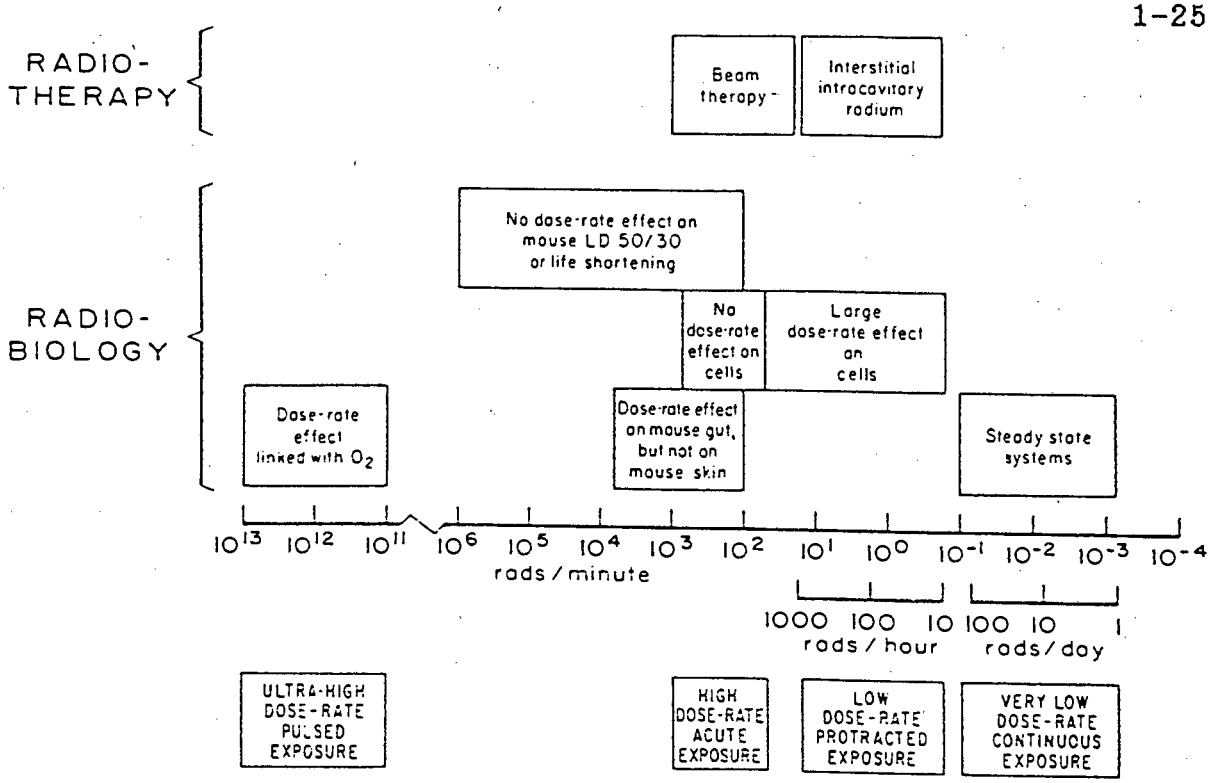

Figure 1.5 The spectrum of dose rates used in radiobiology and radiotherapy (taken from Hall, 1972) (1 rad = 0.01 Gy).

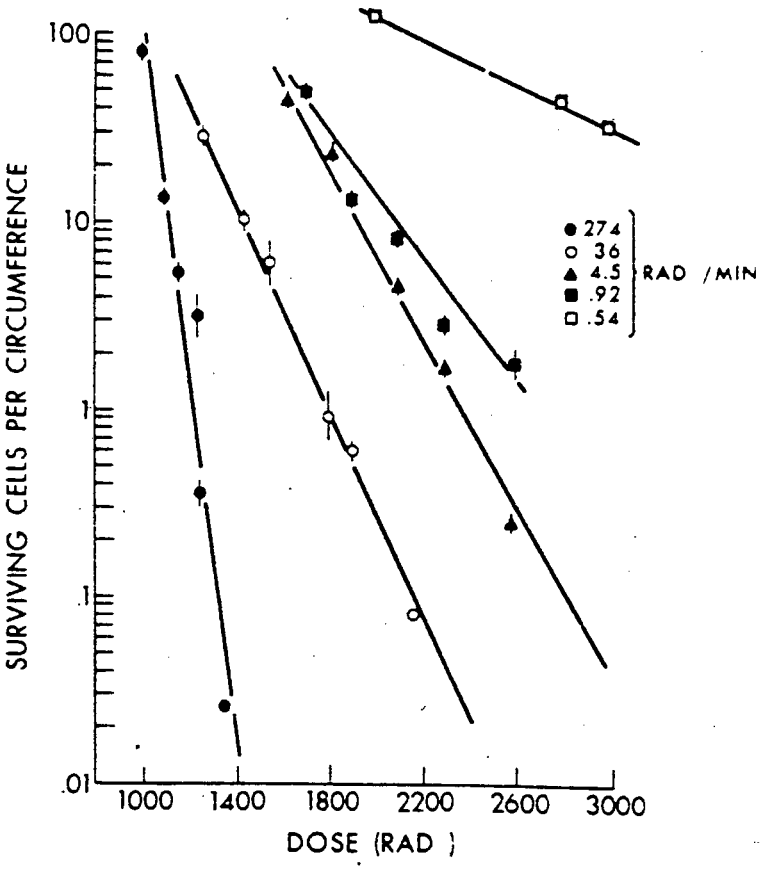

Figure 1.6 Response of mouse jejunal crypt cells irradiated with γ-rays from ^{137}Cs over a wide range of dose rates. (From Fu et al., 1975) (1 rad = 0.01 Gy).

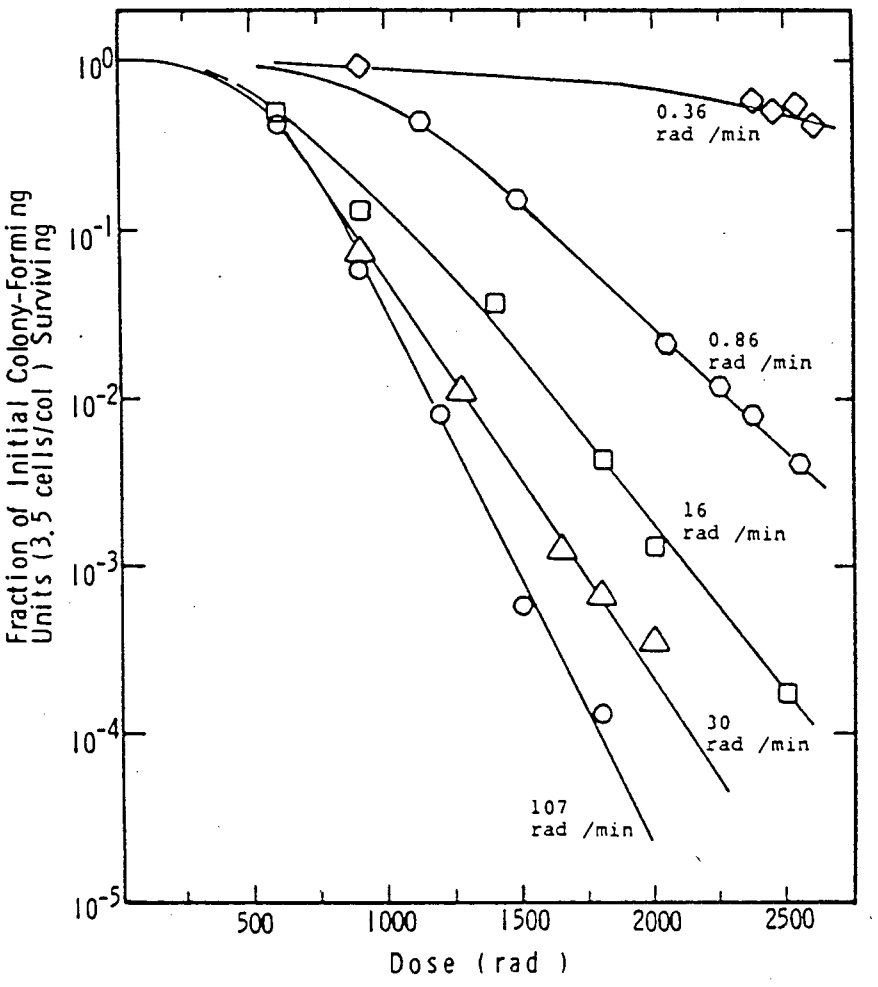

Figure 1.7 Dose response curves for Chinese hamster cells (CHL-F line) grown in vitro and exposed to cobalt-60 ɣ-rays at various dose rates. (From Bedford and Mitchell, 1973) (1 rad = 0.01 Gy).

The effect of very low dose rate irradiation has been extensively studied. A relationship between the cell cycle time and the dose rate necessary to stop cell proliferation has been established. (Mitchell et al., 1979a, b and c; Bedford and Mitchell, 1973; Hall, 1972).

The dose rate effects in the dose rate range from very low dose rates to moderate dose rates (10^{-4} Gy/min to 10 Gy/min, see figure 1.5) are summarised in figure 1.8. As the dose rate is reduced, the survival curve becomes shallower due to the

increased repair of sublethal damage. At very low dose rates, cell proliferation continues during irradiation and causes the survival curve to be even more shallow. As the survival curve becomes shallower, the extrapolation number tends to unity.

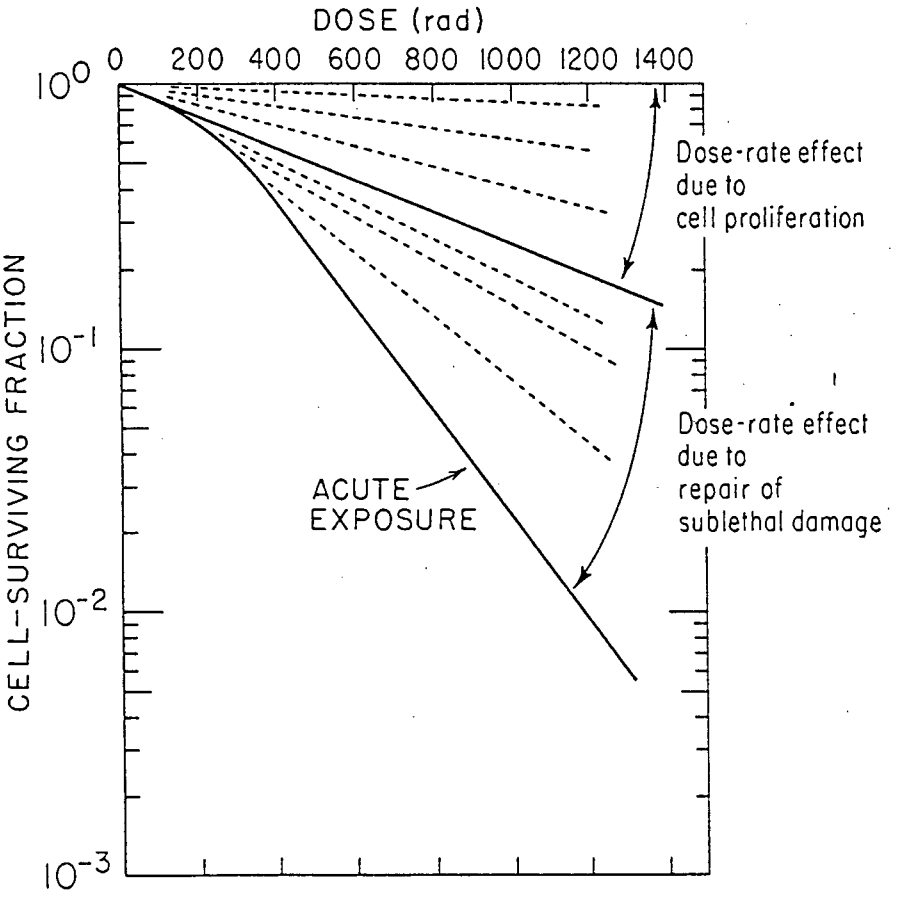

Figure 1.8 Illustrating the dose rate effect due to (a) repair of sublethal radiation damage, and (b) cell proliferation (From Hall, 1978) (1 rad = 0.01 Gy).

The dose rate range from 10 Gy/min to 10^{-4} Gy/s is of special interest because this dose rate range spans the same range used in this work. From the early work in this dose rate range, no dose rate effect was expected. This was demonstrated by Lindop and Rotblat (1963) in a number of *in vivo* systems. They observed little effect for a change of dose rate from 0.8

Gy/min to 1600 Gy/min on the $LD_{50/30}$ in mice irradiated with electrons ($LD_{50/30}$ is the dose required to kill 50% of the irradiated mice within 30 days). Ainsworth et al. (1964) also found no influence on the $LD_{50/30}$ for mice irradiated with gamma rays at dose rates from 1 Gy/min to 10^4 Gy/min. Denekamp and Fowler (1966) found no dose rate effect between 1 Gy/min and 60 Gy/min when scoring skin damage in mice.

The work of Hornsey and Alper (1966), however, showed an unexpected increase in the effectiveness of electron radiation in killing mice within four days when a dose rate of 60 Gy/min was used as compared with a dose rate of 1 Gy/min. This was later confirmed by Hornsey (1970) for mice of a different strain. Hornsey and Bewley (1971) found that dose rates above 60 Gy/min were less effective in killing mice within four days. This decrease in effectiveness was shown to originate from the intracellular oxygen being depleted by the radiation. In this respect, Hornsey and Bewley (1971) note a similar effect to Epp et al. (1968), but at a much lower dose rate (see review of ultrahigh dose rates).

If dose rates above 10 Gy/min are to be used in therapy, the work of Hornsey and Alper (1966) suggests the need for a thorough investigation of a possible dose rate effect on the effectiveness of the radiation in cell inactivation.

At the ultra high dose rate region (above 10^4 Gy/s, see figure 1.5) a dose rate effect is observed that is linked to the

depletion of intracellular oxygen. Epp et al. (1968) have investigated the effect of ultra high dose rate electron irradiation on the survival of *Escherichia coli* B/r at different oxygen concentrations. Their irradiation was done at a dose rate of the order of 10^{10} Gy/s. Their findings are presented in figure 1.9. The survival curves have the usual survival curve shape for oxygenated cells up to a certain "break-away" dose, which is dependent on the oxygen concentration, and then have an anoxic survival curve shape. These results have been explained in terms of a local oxygen depletion by the action of the radiation at a rate which is greater than the diffusion rate of oxygen in these cells. Griem et al. (1969) have shown a similar trend when irradiating Chinese hamster cells with pulsed electrons at dose rates of the order of 10^{7} Gy/s and thus confirm the work of Epp et al. (1968) and the earlier work of Dewey and Boag (1959).

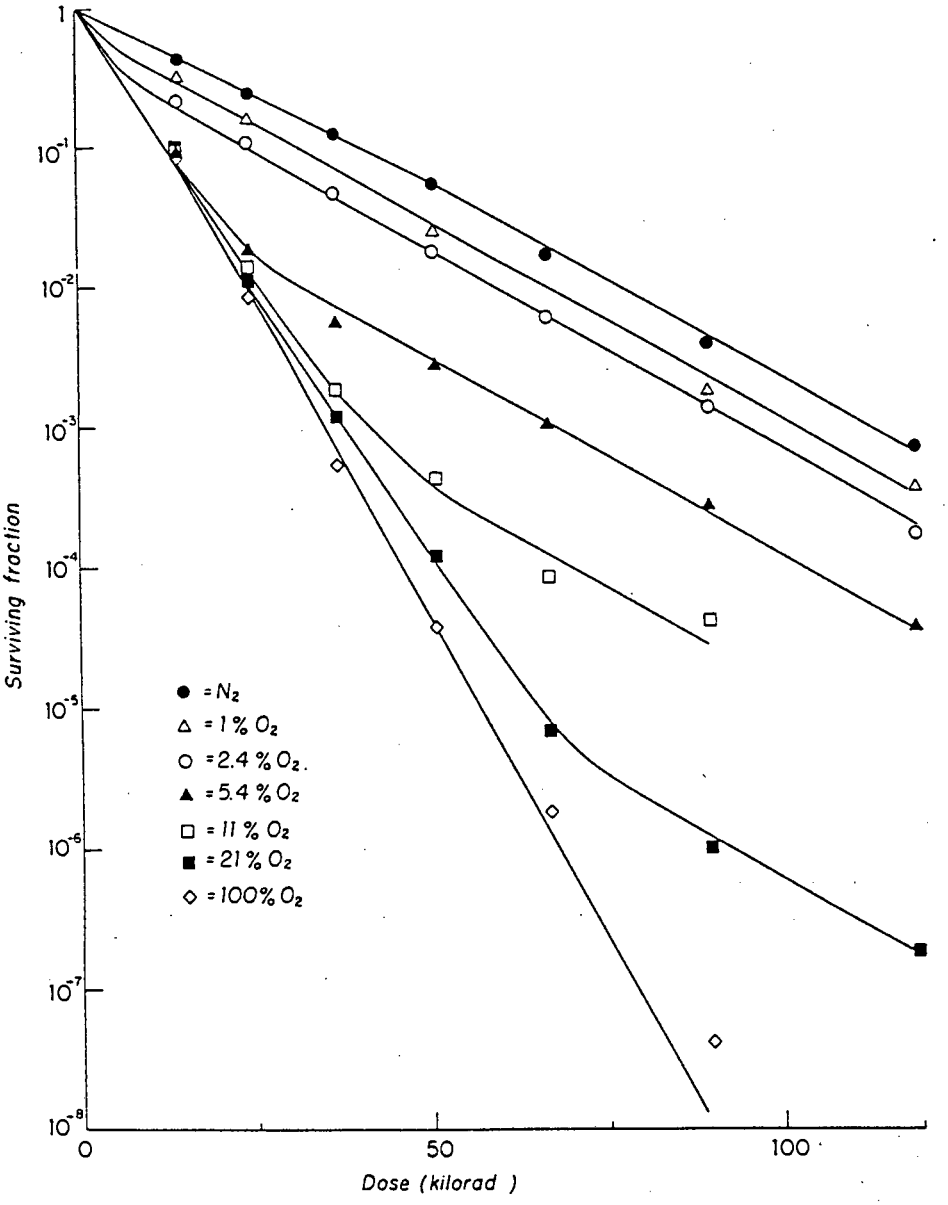

Figure 1.9 Survival curves for *Escherichia coli* B/r irradiated with single short (30 ns) pulses of electrons under various oxygen concentrations. (From Epp et al., 1968) (1 rad = 0.01 Gy).

1.5 THE SCOPE OF THIS WORK

The proton beam used in this work was generated by the Van de Graaff accelerator of the CSIR in Faure, South Africa. An operating proton beam energy of 4.5 MeV was used. Special cell irradiation apparatus was developed and mammalian cell survival curves were measured using Chinese hamster V79-379A cells. The survival curves were measured at dose rates of about 3 Gy/s and 300 Gy/s, and over a dose range from zero to 20 Gy.

The first measured survival curves showed two distinct features:

(1) The low dose rate curve revealed very much higher levels of survival than the high dose rate curve.

(2) In both cases, after an initial typical fall in the surviving fraction up to a dose of about 4 Gy, the survival curves flattened off to a constant surviving fraction of about 10 per cent.

Since these results did not conform to the standard survival curve shape, a number of possible causes were investigated. Firstly, that some of the cells were not being irradiated due to poor sample alignment; secondly, that a radiation dose rate effect, linked to the depletion of intracellular oxygen, was present; thirdly, that the current measuring apparatus was inadequate and hence gave rise to significantly incorrect dose

rates. The latter, however, would not explain the general features of the curves, but would only have an effect on the slopes.

The first effect was tested by making two modifications to the apparatus:

(1) To overcome a possible alignment error, the radiation vessels were made smaller than the beam diameter (15 mm) which was used for the original measurements.

(2) A nickel scattering foil was introduced, at an appropriate place in the proton beam-line, to ensure a homogeneous beam profile. The proton beam profiles were measured using dose verification film.

A control survival curve was measured using cobalt-60 radiation at a dose rate of 4.11 Gy/min (the maximum dose rate available). The resulting survival curve compared well with other work, thus indicating the appropriateness of irradiating V79 cells as monolayers in the specially constructed radiation vessels. Subsequent survival curves measured using proton irradiation were, however, not significantly improved when compared with those measured earlier.

A radiation dose rate effect linked to the depletion of

intracellular oxygen was tested using the hypoxic cell sensitser, misonidazole. The results were inconclusive.

Finally, the current measuring device was tested. The original Faraday cup used was found to be inadequate for measuring the proton beam current. A new Faraday cup was designed and tested. Particle induced x-ray emission (PIXE) was used to confirm that the measured high current to low current ratio was correct. Using the new apparatus, no appreciable quantitative difference between the high and low dose rate survival curves was now observed. However, the earlier problems of unusually high survival levels and a two component slope for the high dose rate survival curve persisted. The survival curves were corrected for the effect of the measured proton beam profiles. The results were then compared with other published work.

The materials and methods as well as the developments are described in chapter 2. The early results which led to the experimental modifications and developments as well as the final results and discussion are presented in chapter 3. Brief conclusions are drawn in chapter 4.

2 CHAPTER TWO: MATERIALS AND METHODS

2.1 CELL IRRADIATION ARRANGEMENT

The experimental arrangement for irradiation consisted of the horizontal proton beamline with a 6.35 μm nickel multiple scattering foil, collimators and a 6.35 μm Havar (see appendix B) exit window, and the cell exposure apparatus, which included a charge collecting Faraday cup, a cell sample holder and shutters for regulating the exposure time. The irradiation arrangement is shown in figure 2.1. The cell samples were contained in specially constructed radiation vessels with 6 μm Mylar bases. The charge collected by the Faraday cup was accumulated with a current integrator and the data was recorded on the National Accelerator Centre's (NAC) data acquisition system. At a later stage of the project, particle induced x-ray emission was also used for current monitoring. Beam profiles were examined with the aid of Kodak X-Omat V dose verification film and a Therados (model RFA-3-50) densitometer.

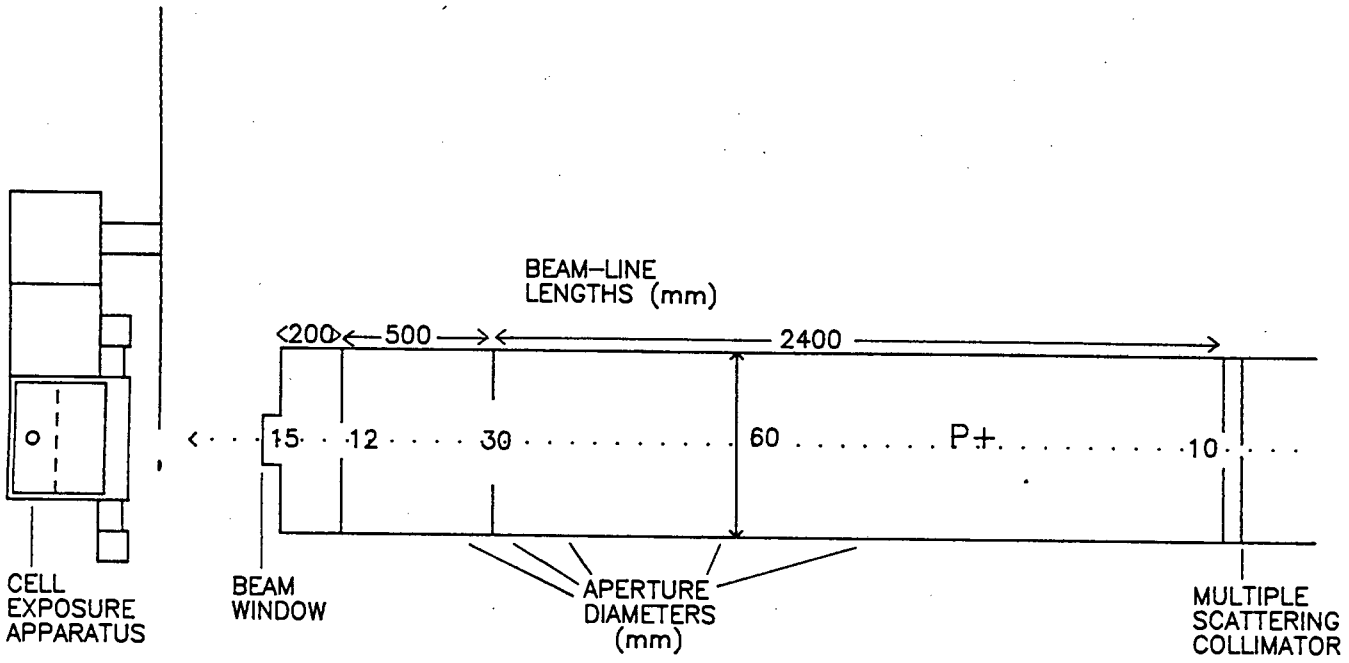

Figure 2.1 The irradiation arrangement showing the proton beamline and the cell exposure apparatus. A thin nickel foil is mounted on the multiple scattering collimator to defocus the beam.

2.2 PROTON BEAM CHARACTERISTICS

The Van de Graaff accelerator, at the NAC in Faure, was operated at a proton energy of 4.50 MeV. Since protons of this energy have a range in water of only 0.3 mm (Janni, 1982), every effort was made to minimise the energy losses along the beam path. This was necessary so that the cells could be irradiated at an energy where the dose delivered would not depend strongly on the proton energy (i.e. in the plateau region of the Bragg ionisation curve). The protons had to pass out of the beamline vacuum through a 6.35 μm Havar exit window and then through an air gap of about 3 cm before passing through a 6 μm Mylar foil before finally penetrating the cells.

At each stage energy is lost.

In radiation experiments, it is desirable for the beam to have a homogeneous dose distribution over the sample area to ensure equal exposure of the target. Initially, the proton beam was defocussed to achieve this, but later a 6.35 μm nickel scattering foil was introduced to spread the proton beam by means of multiple scattering (Perris et al., 1986 and Bettega et al., 1979). This nickel foil was placed at an arbitrary distance from the beam window at first, but was later fixed to a rotary collimator (multiple scattering collimator in figure 2.1) approximately 3 m from the exit window, in accordance with multiple scattering calculations (see appendix C). Beam flatness of ± 0.5% was calculated over the target area. No account was taken of scattering from the beam tube (diameter = 60 mm). Measurements of the beam profile, however, indicated that the beam flatness uncertainty was about ± 20% (see section 3.6, page 3-11).

The 4.50 MeV proton beam lost 287 ± 3 keV in the nickel scattering foil, 276 ± 2 keV in the Havar exit window, 304 ± 5 keV in the 3 cm air space and 83 ± 2 keV in the Mylar before reaching the cells (Janni, 1982). The energy loss in Havar was calculated from a weighted sum of the energy losses in the constituent elements (see appendix B). The final energy of the proton beam at the cell layer was therefore 3.56 ± 0.02 MeV, a beam energy uncertainty of less than 1%. The uncertainties in the thicknesses of the scattering foil and exit window are not

included in the above calculations. If these uncertainties are taken as 10% and the uncertainty in the air gap is taken as 20%, then the final energy of the proton beam at the entrance to the cell layer would have been 3.56 ± 0.07 MeV, an uncertainty of less than 2%. The thickness of the Chinese hamster cells is given by Bird et al. (1980) as 6 μm, while Perris et al. (1986) report 6.3 μm. For a cell thickness of 6 μm (taken as unit density), the energy lost by a 3.56 MeV proton beam is only 61 ± 1 keV (Janni, 1982). If the uncertainty in the cell thickness is as high as 20%, the uncertainty in the final energy of the proton beam would still be less than 2%. Since the energy loss in passing through the cells was small, the proton beam energy did not change significantly, and hence the specific ionisation of the protons was very nearly constant as they passed through the cells. The LET of the irradiating protons was therefore taken as 10.2 ± 0.2 keV/μm (Janni, 1982; Perris et al., 1986; Bird et al., 1980; Wainson et al., 1972).

The possible presence of a low energy proton beam component which was unable to penetrate the cells, was checked by measuring the proton beam current with and without sheets of Mylar foil between the beam window and the Faraday cup. No measureable difference in the measured current was detected even with multiple Mylar sheets totalling about 50 μm in thickness.

The diameter of the 6.35 μm thick beam window was chosen to be

15 mm since it was expected that a larger window of the same material would not have been able to support the vacuum in the beam line.

2.3 DOSIMETRY

The derivation of absorbed dose is relatively simple for low energy proton beams. From the definition of the Gray as one joule of energy absorbed per kilogram of tissue mass, we can derive the dose rate from the proton beam current as:

$$\text{Dose rate} = \frac{L.I.10^6}{\rho.A} \text{ Gy/s} \qquad (2.1)$$

Where L is the LET in keV/μm, I is the proton current in ampere, ρ is the tissue density in g/cm^3 (taken as 1) and A is the proton beam cross-sectional area in square metres.

Since the beam diameter at the sample is 1.50 ± 0.02 cm, the beam area is 1.77 ± 0.03 cm^2, and L is 10.2 ± 0.2 keV/μm, the dose rate is given by:

$$\text{Dose rate} = 5.76 \times 10^{10} \times I \text{ Gy/s} \qquad (2.2)$$

Where I is the beam current in ampere and the uncertainty in the constant (3%) must be added in quadrature to the uncertainty in the current to obtain the final uncertainty in the dose rate.

2.3.1 CURRENT MEASUREMENT USING FARADAY CUPS

The proton current was measured by means of a graphite Faraday cup, K. In the cell exposure system as a whole, it was located behind aperture G as shown in figure 2.13 on page 2-22. Figure 2.2 and 2.3 show photographs of the Faraday cup in the sample holder and the sample holder installed in the cell exposure apparatus. Figure 2.4 is a diagram of the cell exposure apparatus showing the disc shutter and the sample holder which slides behind the disc shutter. Figure 2.5 gives the block diagram of the electronics for the measurement of current and the recording of these measurements. The current was recorded every second in successive multichannel analyser (MCA) channels for one minute and printed out for later processing to determine the stability of the beam current.

The graphite Faraday cup is shown diagramatically in figure 2.6. This Faraday cup was regarded as adequate for the initial proton experiments because a calculation of the number of backscattered protons revealed that only about 0.001% of the incident protons would be backscattered out of this cup (see appendix E). Consistently inexplicable results (see chapter 3) as well as clear differences in the darkness of dose verification film exposed to the beam for the same total dose but at different dose rates, led subsequently to the questioning of the reliability of the graphite Faraday cup.

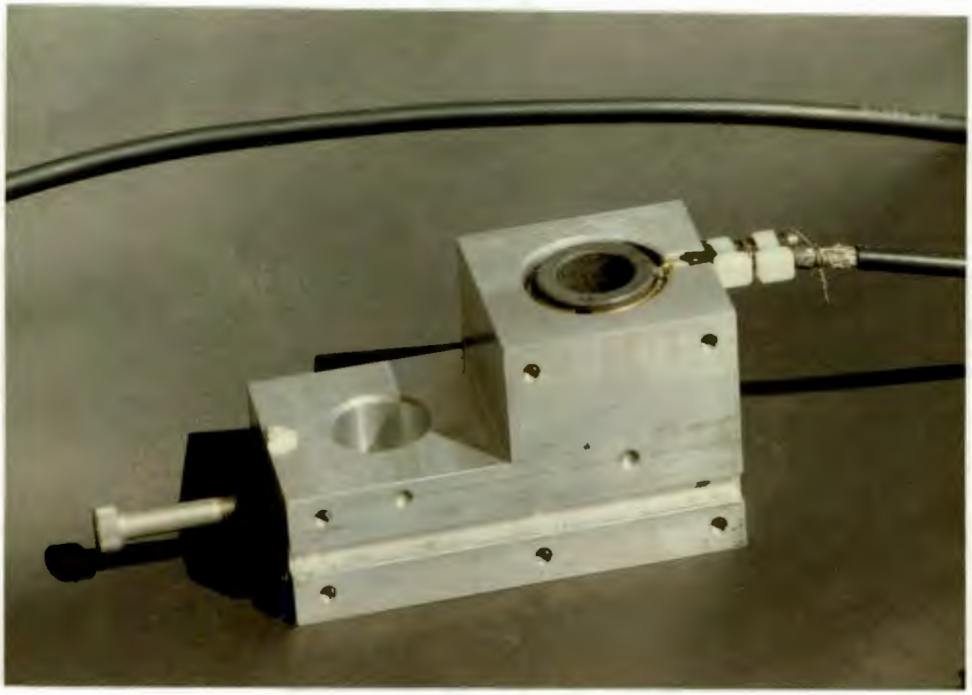

Figure 2.2 The sample holder with the graphite Faraday cup installed.

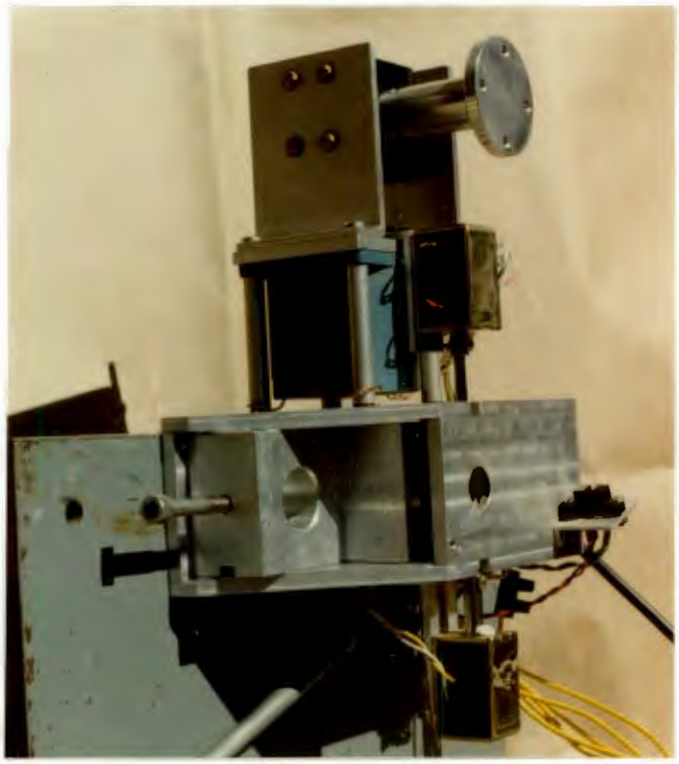

Figure 2.3 The sample holder installed in the cell exposure apparatus. In this position the Faraday cup is aligned behind the final beam collimator (G in figure 2.13). The disc shutter has been removed for clarity.

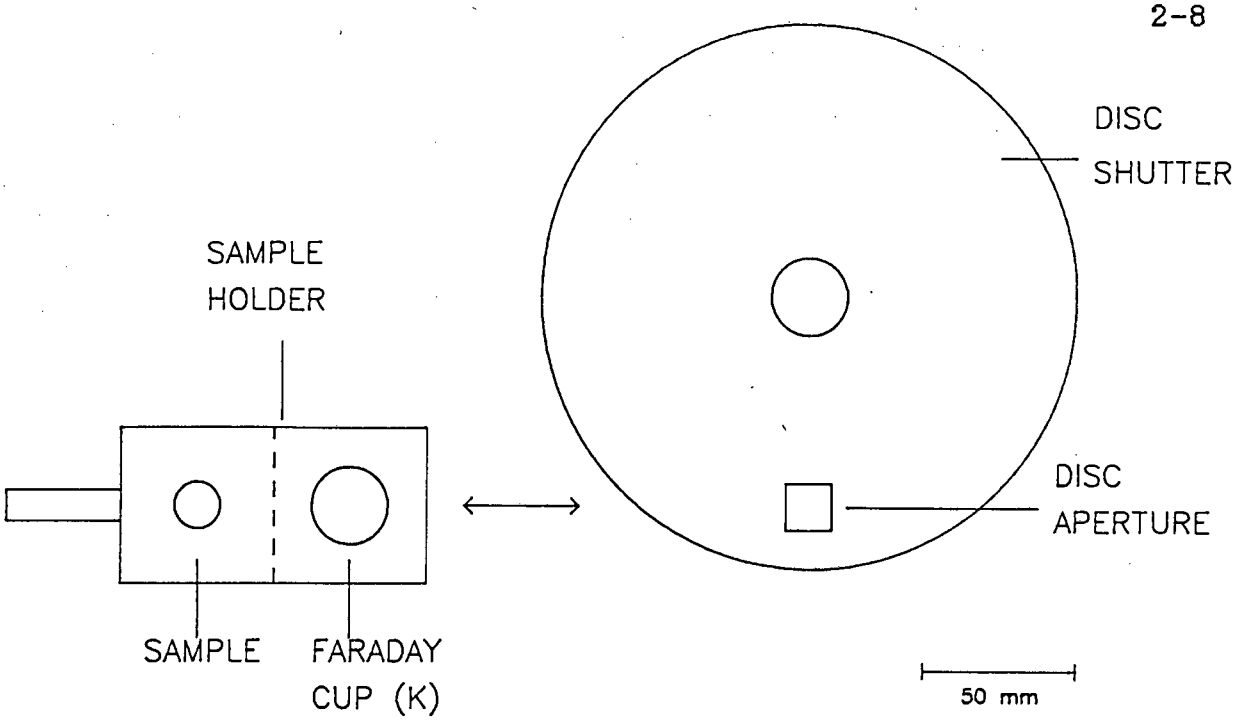

Figure 2.4 A diagram showing the sample holder, which contains both the sample and the graphite Faraday cup, and the disc shutter. The sample holder can slide behind the disc shutter as shown. The proton beam is directed into the page at the disc aperture.

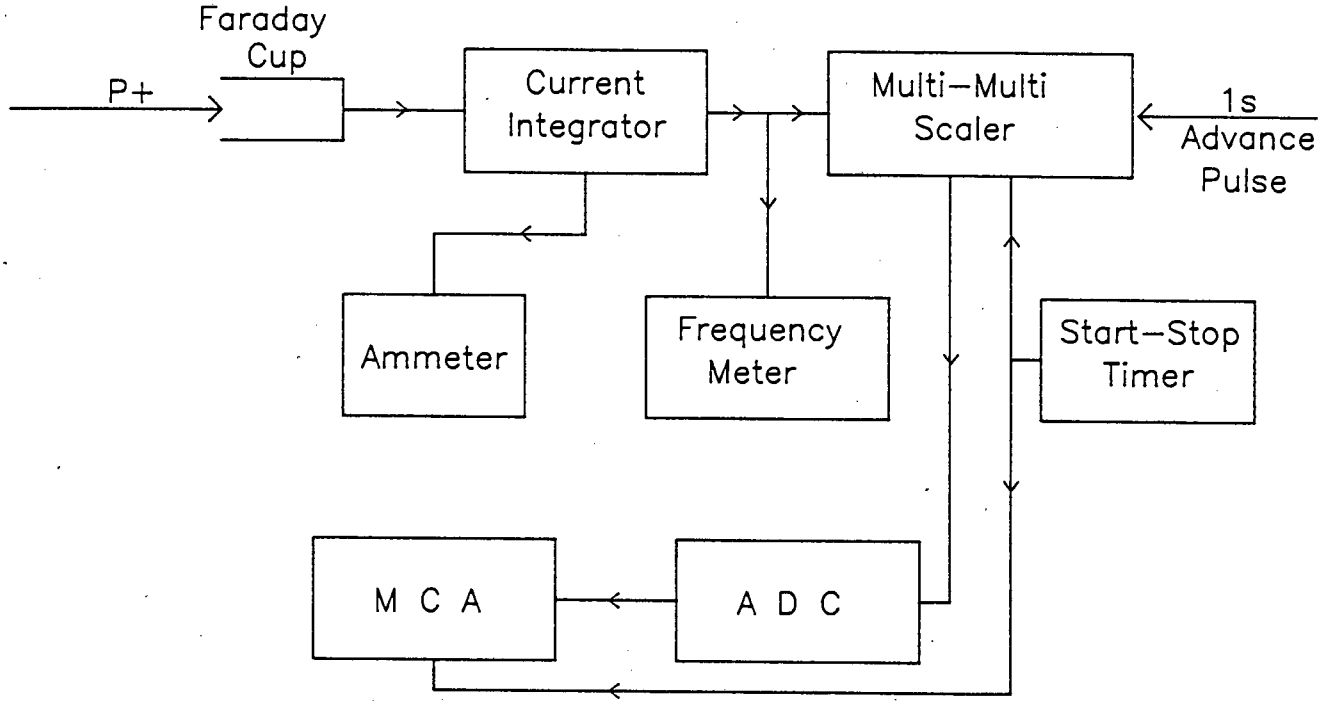

Figure 2.5 Block diagram showing the electronics for current measurement.

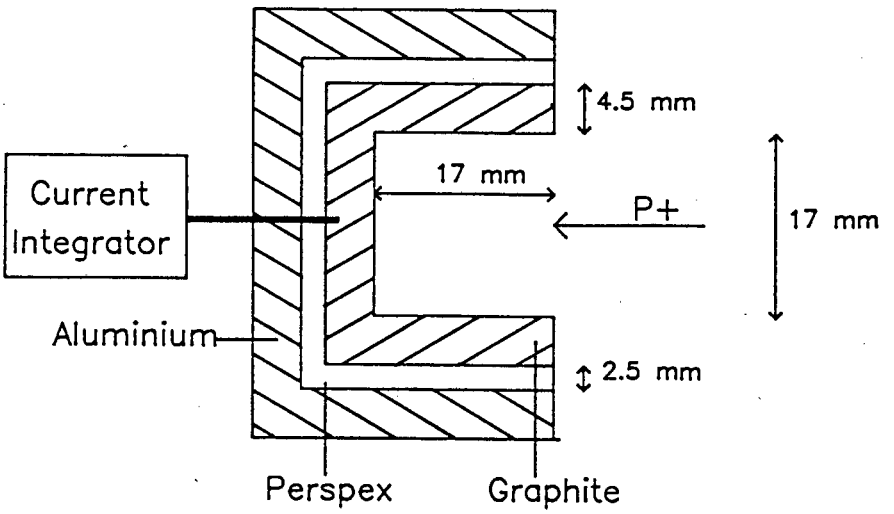

Figure 2.6 Diagram of the graphite Faraday cup. The perspex insulates the cup from the aluminium holder.

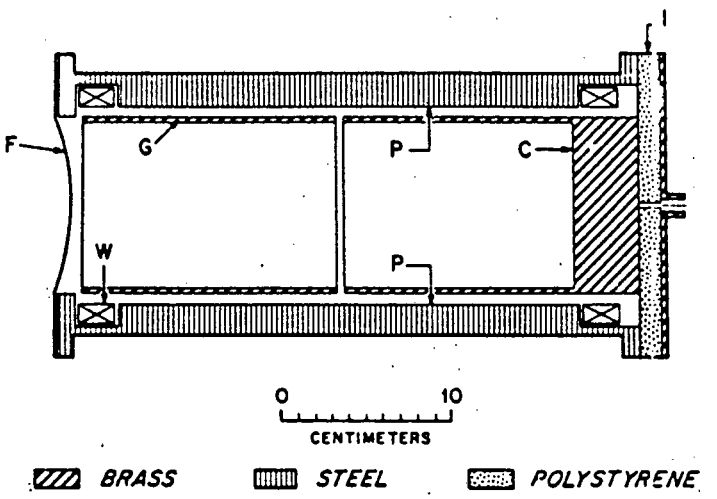

Figure 2.7 A diagram of the Harvard Faraday cup. C is the collecting cup, F is the entrance window, G is a guard ring for electric field application, W are windings for magnetic field application, P is the steel casing and I is a polystyrene insulator (taken from Verhey et al., 1979).

England (1974) points out the many difficulties associated with the measurement of particle beam currents in air with a Faraday cup, the most significant being that of ion pair formation as the charged particle passes through the air and electrons leaving or entering the Faraday cup. Although his design considerations were beyond the scope of this work, a Faraday cup made of aluminium with an inner diameter of approximately 2.5 cm and a length of approximately 7.5 cm, was constructed to measure the proton beam current inside the vacuum line (see figure 2.8). The length to diameter ratio of this Faraday cup was chosen to match that of the Faraday cup of Verhey et al. (1979), which was developed for the 160 MeV proton beam at Harvard University (see figure 2.7). The guard ring and magnetic field windings are for electron suppression. Their work showed that at zero guard ring potential, zero magnetic field and spoiled vacuum, this Faraday cup measured the correct beam current. From the secondary electron emission data for helium ions (Matteson and Nicolet, 1979), it was possible to estimate the number of secondary electrons emitted when the proton beam strikes the base of the aluminium Faraday cup, as approximately 1 per proton (Peisach, 1988) The solid angle of the aluminium Faraday cup was only 0.085 steradian (0.0068 of 4 pi). Secondary electron emission should therefore not affect the measurement of the current by more than 1% (0.0068 x 100).

On consideration of the above, and bearing in mind the fact that the important parameter in this work was the ratio of the high to low current and not accurate absolute current, the

aluminium Faraday cup was accepted as satisfactory for the measurement of the beam current.

The aluminium Faraday cup shown in figure 2.8 was constructed in such a way as to act as both the beam window and a Faraday cup. The base of the Faraday cup was made of 6.35 μm Havar to act as the beam window, while a small removable aluminium cap stopped the beam and allowed the current to be measured. This Faraday cup is shown installed on the beam line in figure 2.9 with the removable cap fitted.

The need for suppression of electrons entering the Faraday cup was tested by applying a voltage (-1000 V) to the insulated 12 mm collimator which is situated 200 mm from the beam window (see figure 2.1). The test produced no measureable effect on the current measurement obtained with the internal aluminium Faraday cup.

Particle induced x-ray emission spectroscopy (PIXE) was also used to monitor the beam current and provide a reliable measurement of the high to low current ratio, which was then compared with the same ratio as measured by the aluminium Faraday cup.

Figure 2.8 The internal aluminium Faraday cup fitted to the mounting flange.

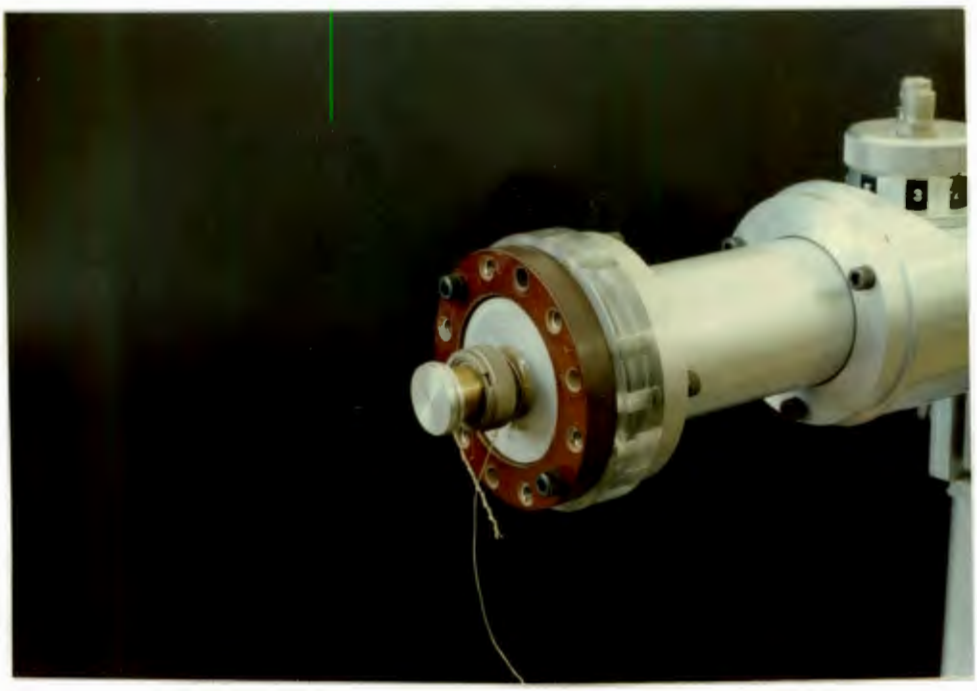

Figure 2.9 The aluminium Faraday cup fitted at the end of the beam line. The beam window is closed with the removable beam stop. The Faraday cup is insulated from the beam line by the thick perspex spacer.

2.3.2 CURRENT MONITORING WITH PARTICLE INDUCED X-RAY EMISSION

An aluminium tube, the same length and diameter as the aluminium Faraday cup, with its distal end machined at an angle of 45° to the tube, was manufactured. A 6.35 μm thick nickel foil covered the end of the tube (see figure 2.10).

When protons strike nickel foil, they cause the nickel to radiate characteristic x-rays. The most dominant x-rays are the 7.472 and 8.265 keV x-rays which come from the K-alpha and K-beta transitions respectively (see figure 2.11). Spectra of these peaks were accumulated at the high and low current settings. The count rate at which the spectra were collected was easy to compute from the detector live time. By comparing the count rates, a reliable ratio of the high to low current for the proton beam was established. The electronics necessary for PIXE detection is shown in figure 2.10.

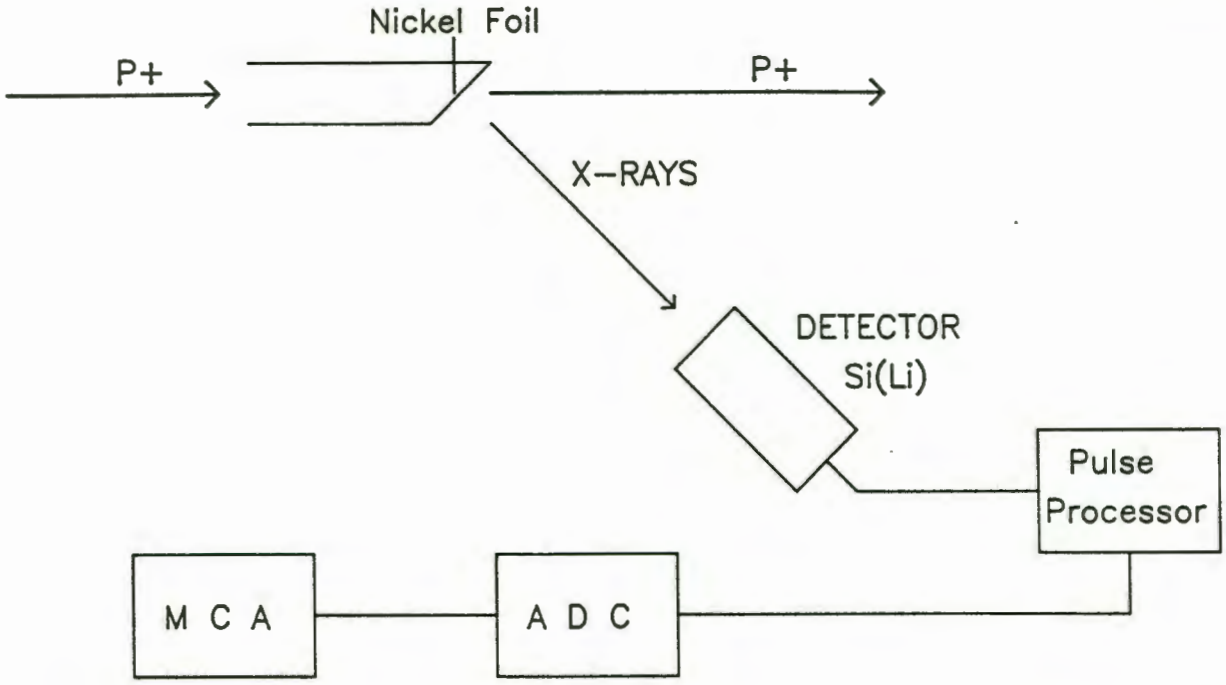

Figure 2.10 Block diagram of the PIXE setup, showing the geometry and the electronics for collecting the data.

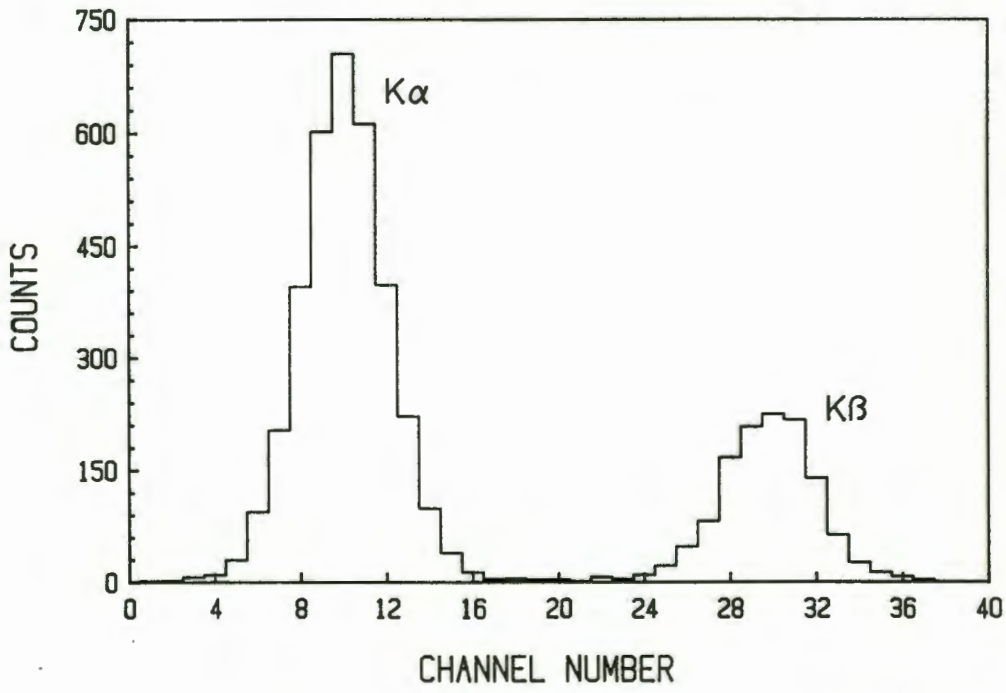

Figure 2.11 A typical nickel PIXE spectrum. The spectrum was integrated, over the range of channels shown, to determine the total number of counts (4644 counts in this case). Since this spectrum was collected in 54 seconds, the average count rate was 86 c/s.

2.4 DOSE RATE ADJUSTMENT

The dose rate ratio desired for this work was approximately 100. Therefore, the ratio of high to low current had to be about 100 as well. It is undesirable to change the proton current by changing the settings on the Van de Graaff accelerator, since this can affect the shape of the beam and could produce unpredictable results. The problem was solved by mounting the nickel scattering foil (see section 2.1) on a rotary collimator. The rotary collimator was designed to have three collimator settings:

(1) A 5 mm aperture covered with the nickel foil.
(2) A 0.5 mm aperture also covered with the nickel foil.
(3) A 5 mm aperture without the nickel foil.

Aperture (3) above was used for beam centering since it allowed a much higher current to be measured at the beam window. Multiple scattering in the nickel foils covering apertures (1) and (2) above provided a more uniform beam profile. Since the ratio of the areas of the first two apertures was 100, these apertures provided the high and low current settings.

2.5 PROTON IRRADIATION PROCEDURE

Prior to irradiating the samples, the beam was correctly aligned and the appropriate collimator was selected to allow for high or low current exposure (see section 2.4). The current was monitored and the dose rate calculated using equation 2.2 (dose rate = $5.76 \times 10^{10} \times I$ Gy/s, I measured in ampere).

The sample exposure times (or disc shutter frequencies) for the required doses were calculated and entered into the appropriate column on the data sheet shown in figure 2.12 (see sections 2.7.2 and 2.7.3). The samples were then exposed for periods of time as close to the times calculated as possible. The actual exposure times were recorded after each sample was irradiated. Prior to and immediately after each vessel was irradiated, the proton beam current was monitored for a full minute and the 120 current measurements thus obtained were printed out and later analysed to determine the statistical uncertainty. From these current readings the dose rate, at the time of irradiation, for each sample was calculated. These, together with the recorded actual exposure times, allowed for the calculation of the actual dose given to each sample.

Since all the above current readings were measured with the graphite Faraday cup, this cup was calibrated against the internal aluminium Faraday cup and the PIXE count rate (see section 2.3.2). The ratio of the PIXE count rates was used as

a check of the ratio of the high to low current measurements.

The above procedure was repeated after the collimator had been rotated to select the alternate current setting.

The analysis of the current data revealed a random uncertainty in the current measurements of about 1%. By combining the uncertainty in the exposure times, the random uncertainty in the dose precision was found to be not more than 5%.

EXPERIMENTAL DATA

DATE Dec 1986
DOSE RATE 240 Gy/s
RADIATION Protons
ENERGY 4.5 MeV
CURRENT

REMARKS

NO	(Gy) DOSE aim	(Gy/s) DOSE RATE	(Gy) DOSE act	IRR TIME aim (s)	IRR TIME act (s)	(Hz) FREQ aim	(Hz) FREQ act	CELL no/ml X10⁴	CELL FOR aim	NO PLATING act	NO OF COLONIES	PLATING EFFICIENCY	SURVIVING FRACTION
0	0	240	0					18.0	200	167 (10%)	157 (6%)	0.90 (13%)	1.0
1	2.0	240	2.17	0.00833	0.0090	6000	5530	16.9	300	263 (10%)	147 (8%)	0.56 (13%)	0.62 ± 0.11
2	4.0	234	4.24	0.0167	0.0181	3000	2759	12.1	500	477 (9%)	114 (9%)	0.24 (13%)	0.27 ± 0.05
3	6.0	230	6.24	0.025	0.0271	2000	1843	13.8	1000	1074 (8%)	218 (7%)	0.20 (11%)	0.22 ± 0.04
4	8.0	241	8.75	0.033	0.0363	1500	1377	18.4	2000	1780 (12%)	288 (6%)	0.16 (13%)	0.18 ± 0.03
5	10.0	229	10.38	0.042	0.0453	1200	1103	14.6	4000	3938 (11%)	700 (7%)	0.18 (13%)	0.20 ± 0.04
6	12.0	237	12.99	0.05	0.0548	1000	912	17.3	6000	5700 (10%)	900 (7%)	0.16 (12%)	0.18 ± 0.04
7	20.0	235	21.10	0.083	0.0898	600	557	16.5	8000	6900 (10%)	367 (5%)	0.05 (11%)	0.06 ± 0.01

Figure 2.12 A reduced copy of the experimental data sheet which was useful for recording the relevant data during experiments. Typical data is shown to illustrate the use of the sheet (from figure 3.10, page 3-18). The numbers in brackets are percentage uncertainties.

2.6 BEAM PROFILE MEASUREMENTS

Standard film dosimetry was used to measure the proton beam profiles for two reasons:

(1) The small beam area makes the use of finite size detectors very difficult.

(2) Film has a fast response, while other methods take much longer to collect the profile, allowing time for beam fluctuations to "smooth out" the actual beam profile.

The use of film presented its own problems: Densitometer detectors have an area of about 3 mm^2, resulting in an undesirable averaging of the recorded densities over a small beam area. There were also edge effects as the detector moved onto the exposed area. This made the profile seem worse at the edge than it really was. Ideally the detector area should be very much smaller than the area to be scanned, which was not the case in this work.

The film chosen for this work was Kodak X-Omat V. This film is the standard film used for dose verification in radiotherapy. Since the X-Omat V film is packaged in a large envelope, it was cut up in a dark room and covered with tin foil (lightweight domestic) to prevent light from entering. These films were exposed to the proton beam at suitable times between

irradiating the samples. At least four films were exposed at each current setting. The films were then developed using an automatic film developing system which ensured that the films were developed uniformly. The developed films were then scanned on a Therados densitometer (model RFA-3-50). The densitometer scans were digitised using a HP86 microcomputer and were plotted in histogram form.

Before the Kodak X-Omat V film could be used to measure the proton beam profiles, it had to be calibrated in a proton beam. A number of films were prepared and exposed to the proton beam for a range of times from 0.1 s to 1.5 s. The darkest film was scanned and the densitometer was set to read a density of 100 (arbitrary units). The rest of the films were scanned and the maximum density of each was recorded. The density was then plotted against exposure time and analysed to determine the film's response function.

2.7 THE CELL EXPOSURE SYSTEM

The cell exposure system, shown in figure 2.13, can be divided into three parts: the sample holder, the beam shutters and the electronic control units.

2.7.1 THE SAMPLE HOLDER

The sample holder is shown in figure 2.2 on page 2-7 and in figure 2.13 where it is labelled J. The holder slid on a guide rail inside the exposure apparatus and had two locating positions. The one position aligned the sample, inserted in hole L, with the beam and the other aligned the Faraday cup K with the beam. The hole which accomodated the sample was precision drilled to fit the size of the white caps on the Falcon 3033 test-tubes which were used as the radiation vessels. A simple press fit allowed good reproducible alignment of the sample and the proton beam. The sample holder was designed to position the cell layer at the same distance from the beam window as the base of the Faraday cup.

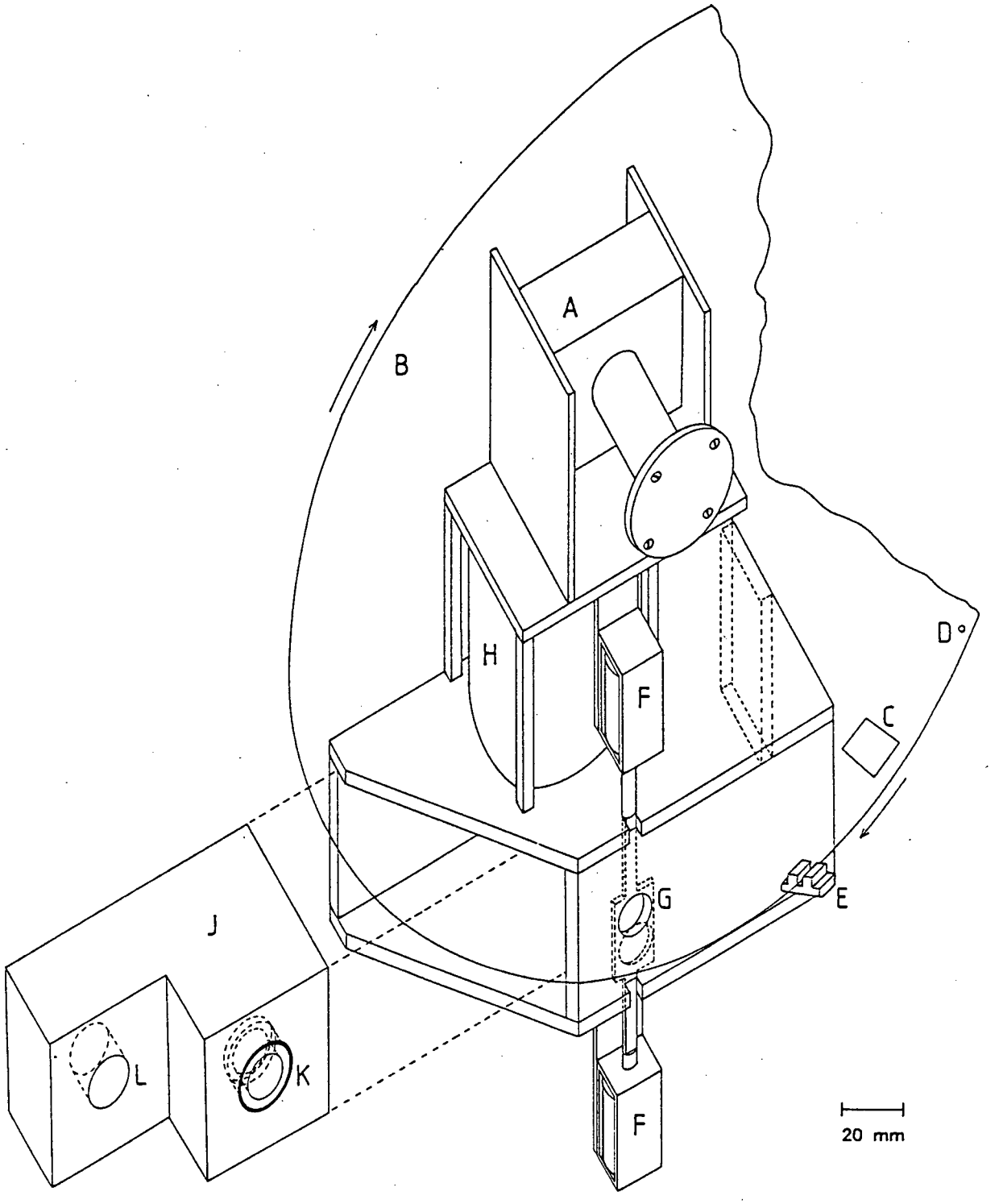

Figure 2.13 The cell exposure system. A the gearbox, B the rotating disc, C the disc aperture, D the sensing hole, E the sensor, F the solenoid shutter, G the final beam aperture, H the stepper motor, J the sample holder, K the Faraday cup, L the sample locating hole.

2.7.2 THE BEAM SHUTTERS

There were two beam shutters, the solenoid shutter and the disc shutter, both shown in figure 2.13.

2.7.2.1 THE SOLENOID SHUTTER - FOR LONG EXPOSURES

The solenoid shutter was simply a piece of stainless steel about 0.5 mm thick which slid in a sleeve behind the beam defining aperture G. The movement of this shutter was controlled by two electric solenoids F, which were operated by an electronic control unit and permitted exposure times ranging from 1 to 99 s, with an uncertainty of 0.15 s. This shutter was only used for exposure times greater than 1.5 s, shorter exposure times were achieved with the disc shutter.

2.7.2.2 THE DISC SHUTTER - FOR SHORT EXPOSURES

The disc shutter consisted of a large disc B (1 mm thick aluminium) which rotated in the direction shown in figure 2.13. This shutter was controlled by a stepping motor H and gearbox A. The stepping motor produced 200 steps per revolution, while use of a 15:1 gearbox caused the system to require 3000 steps per revolution. Since the maximum dose rate envisaged for this work was to be nearly 300 Gy/s, with a minimum dose delivered of about 3 Gy, exposure times of the order of 0.01 s were required. To achieve this, the aperture cut into the disc had a width 1/60 of the circumference of the disc. It was also important that this hole was 15 mm wide, so that the disc could

be stopped with the disc aperture C aligned with aperture G for current measurement (see figure 2.13). This was achieved with a disc approximately 290 mm in diameter. The disc shutter provided exposure times with an uncertainty of less than 1%.

2.7.3 THE ELECTRONIC CONTROL UNITS

The stepping motor was driven by a stepping motor drive connected to a square pulse generator with a variable frequency output. Since the disc requires 3000 steps per revolution and the aperture is 1/60 of the circumference, only 50 steps are required for aperture C to pass a given point. Therefore a required exposure time, t, is given by:

$$t = \frac{50}{f} \qquad (2.3)$$

where f is the square pulse generator frequency in Hertz.

It was necessary for the disc to stop in the "open" position for current measurement. This was achieved by means of a small hole, D, in the disc and a sensing device, E.

Both the solenoid and disc shutters were controlled by an electronic control unit (NAC VDGG 84-1) which provided exposure times with both shutters automatically.

2.8 THE IRRADIATION VESSELS

A proton beam energy of about 3.6 MeV and a beam cross-sectional area of about 1.77 cm^2 required the construction of special radiation vessels.

Falcon 3033 sterile test-tubes were cut off 35 mm from the top. The upper 35 mm of the test-tubes and the white caps were retained, while the lower sections were discarded. The internal diameter of these tubes was 14.5 ± 0.2 mm which matched the beam diameter of 15.0 ± 0.1 mm very well. Small discs, about 18 mm in diameter, of 6 μm thick Mylar were glued to the open base of the test-tube using Bostik Silicone Marine Sealer (see figure 2.14). V79 cells are known to attach to Mylar as with other plastic tissue culture vessels (Bird et al., 1980; Wainson et al., 1972). Care was taken in the construction of these vessels to ensure that the glue did not spread onto the inner surface of the Mylar.

As a result of problems with the preliminary measurements (see chapter 3), these vessels were subsequently modified by inserting a close fitting perspex tube to reduce the inner diameter to 11.0 ± 0.1 mm. Much greater care was taken in the construction of these vessels which resulted in a very neat inner surface with virtually no glue seeping onto the inner surface of the Mylar. After construction, the vessels were soaked in a 5% $NaHCO_3$ solution and were sterilised before use. Figure 2.15 summarises the construction procedure of these

vessels.

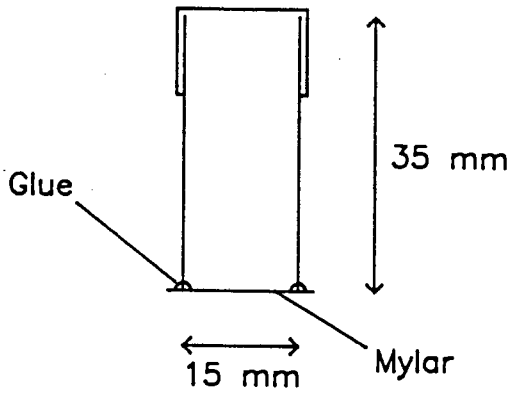

Figure 2.14 The irradiation vessel which was made from the Falcon 3033 test-tube. The beam enters from the bottom.

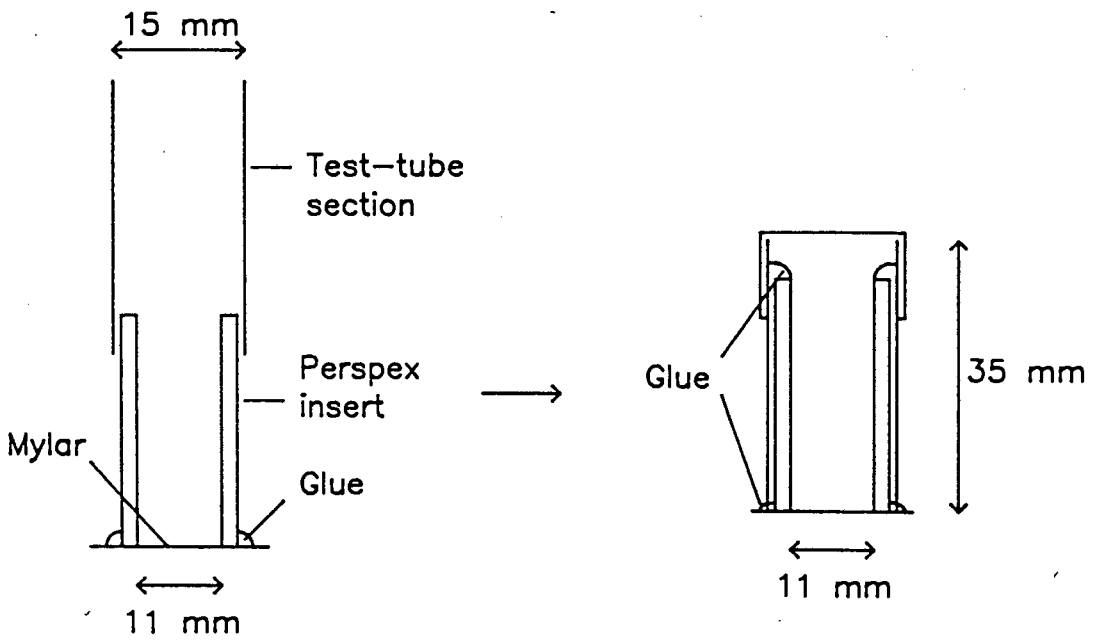

Figure 2.15 The construction of the modified irradiation vessel.

2.8.1 IRRADIATION VESSEL STERILISATION

(i) Vessels and caps were soaked in a 10% solution of 7X (a tissue culture detergent) for approximately 24 hours.

(ii) The vessels and caps were then rinsed thoroughly with tap water until all the detergent was rinsed out. The vessels were then rinsed in distilled water at least three times and left to soak in distilled water for up to 24 hours.

(iii) The vessels were then rinsed in alcohol (methanol or ethanol), before being left to dry in a sterile cupboard.

(iv) When the vessels were thoroughly dry, the lids were screwed on tightly and the vessels were stored until required.

(v) Just before using the vessels, they were rinsed once in cell culture medium (MEM).

The above sterilisation procedure was tested by incubating cells in the vessels for a number of days and monitoring them for any possible contamination.

2.9 CELL CULTURE PROCEDURES

The cells used in this work were the Chinese hamster lung fibroblast line, V79-379A. The doubling time was about seven hours (see appendix A). The cells were grown in stock cultures in T-75 tissue-culture flasks at 37 °C in a humidified 5% CO_2, 95% air atmosphere. The growth medium was Ham's Minimum Essential Medium (MEM), supplemented with 10% foetal calf serum and antibiotics: Penicillin (100 U/ml), Streptomycin (100 µg/ml) and Tylocin (0.5%). The cells attached to the base of the culture vessel where they grew as a monolayer. They were then detached with trypsin (0.5% in 1 ml) and the cell concentration was determined with the aid of a haemocytometer. The required cell concentration was then prepared by dilution of the stock suspension.

The cells were placed into the irradiation vessels 24 hours before they were due to be irradiated. This gave ample time for the cells to attach to the Mylar bases of the vessels and to begin normal exponential growth. To ensure exponential growth, an optimum number of cells needed to be placed in the radiation vessels. This optimum number was chosen, with the aid of the growth curve in Appendix A, so that the cells were approaching confluency, but not confluent (covering the entire base of the vessel), at the time of irradiation. The number of cells chosen was between 50 000 and 60 000 (see appendix A).

The vessels were incubated in a humidified 5% CO_2 air

atmosphere at 37 °C overnight. Early the next morning, the vessel lids were tightened and they were placed in their holding rack in an ice box and transported 25 km from Tygerberg Hospital to the N.A.C. in Faure.

After the samples had been irradiated, they (including the unirradiated control vessels, one per dose rate experiment) were transported back to the Tygerberg Hospital.

The growth medium was decanted from each vessel which was then rinsed with PBS (Phosphate Buffered Saline: NaCl, 10 mM; $Na_2H(PO_4)2H_2O$, 1 mM; KCl, 0.3 mM; $KH_2(PO_4)$, 0.1 mM; pH=7.3). A small amount of trypsin (5% in 0.1 ml) was added to each vessel to free the cells attached to the Mylar. Once the cells were free, they were suspended in about 1 ml of growth medium. The cell concentration was determined for each vessel by counting the number of cells per unit volume with a haemocytometer and using Poisson statistics to determine the uncertainty. The cell concentrations were then diluted according to the expected level of survival and plated into tissue culture flasks (T25) in duplicate. These flasks were then incubated for 4-5 days to allow for colony formation.

Once the colonies were large enough to be counted, they were fixed and stained for easy visibility with amido black stain (0.01% in 20% acetic acid, 20% methanol and 60% water). The resulting colonies were counted to determine the surviving fraction of cells and once again, Poisson statistics were used

to determine the uncertainty. Only groups of cells having 50 cells or more were counted as a colony. (This is the standard procedure for cell survival experiments. See Elkind and Whitmore, 1967; and Bettega et al., 1979). The surviving fraction is calculated as follows; the number of colonies in a flask is divided by the number of cells plated into that flask. This gives the plating efficiency (expressed as a fraction in figure 2.12). The surviving fraction is then obtained by normalising the plating efficiency data, so that the zero dose point has a surviving fraction of one. A sample data sheet containing all the relevant data, including the unirradiated control data and the uncertainties, is presented in figure 2.12. The unirradiated control samples were exactly the same as the irradiated ones and were transported and processed in exactly the same way.

2.10 IRRADIATION PROCEDURE WITH COBALT-60

A survival curve was measured using cobalt-60 gamma radiation, from an AECL Theratron, in the dose range up to 10 Gy, at the maximum dose rate of 4.11 Gy/min. The irradiation was carried out using the same radiation vessels as for the proton irradiation. The time between packing the samples into their transport case and irradiating them was the same. The time between irradiation and reprocessing was also the same as for the proton experiments. The only difference was the radiation source and the dose rate.

The irradiation was carried out at the Karl Bremer Hospital in Bellville. The dosimetry was performed by using a Farmer ionisation chamber (cylindrical, volume = 0.6 ml, type 2505/3) according to the Hospital Physicists Association protocol (HPA, 1983). The field size was 15 cm x 15 cm and the source to sample distance was about 45 cm. The dose was calculated according to the following equation:

$$D = \frac{R}{100}\left(\frac{760}{P} \times \frac{T}{293}\right) \times N \times C \qquad (2.4)$$

where: D = the dose (Gy).

R = the instrument reading.

T = the absolute temperature (K).

P = the atmospheric pressure (mmHg).

N = ionisation chamber calibration factor (supplied by the CSIR).

C = a conversion factor (from exposure to absorbed dose, 0.951; HPA, 1983)

2.11 THE OXYGEN DEPLETION TEST

One interpretation of the shape of the survival curves obtained in this work, was that the intracellular oxygen was being depleted as a result of the high proton irradiation dose rate. This was prompted by comparing these survival curves with those of Epp et al. (1968) presented in figure 1.9 on page 1-30. To test this hypothesis, two sets of samples were prepared, one set having had misonidazole added to the medium ten minutes

prior to irradiation, the other without. The concentration of misonidazole in the medium was about 4 mM. Misonidazole is known to sensitise cells that are temporarily depleted of oxygen as a result of ultra high dose rate irradiation (Michaels et al., 1981; Michaels, 1982). The two sets of samples were irradiated at the same dose rate according to the procedure outlined above. The survival curves were measured and compared.

3 CHAPTER THREE: RESULTS AND DISCUSSION

3.1 INITIAL RESULTS

The initial experiments were conducted with the 15 mm diameter irradiation vessels (see section 2.8, page 2-25). Proton beam homogeneity was achieved by defocussing the beam and the beam current was changed by modifying the accelerator settings. The dosimetry was performed with the graphite Faraday cup.

The survival of V79 cells in response to 3.6 MeV proton irradiation at high and low dose rates in two experiments is illustrated in figures 3.1 and 3.2. In neither case does the surviving fraction fall much below 0.1, even though the proton dose levels extended to above 15 Gy. In figure 3.2 the surviving fraction for high and low dose rates approaches a survival level of 0.5 and 0.15 respectively. The experimental data in figure 3.1 seem to indicate that the high dose rate survival curve has a two-component slope with the initial region, from 0 to 5 Gy, being fairly steep, while the region above 5 Gy has a shallower slope. Both experiments show a significant difference between the high and low dose rate survival, with the high dose rate irradiation being more effective than the low dose rate irradiation.

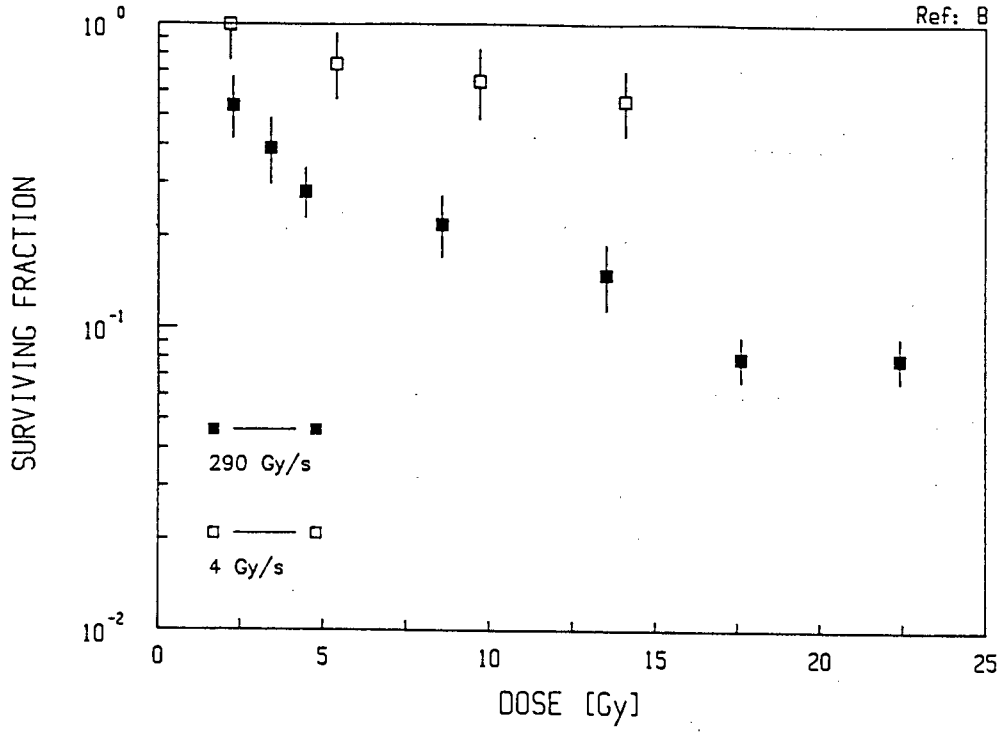

Figure 3.1 Survival data for V79 cells exposed to 3.6 MeV protons at high and low dose rate.

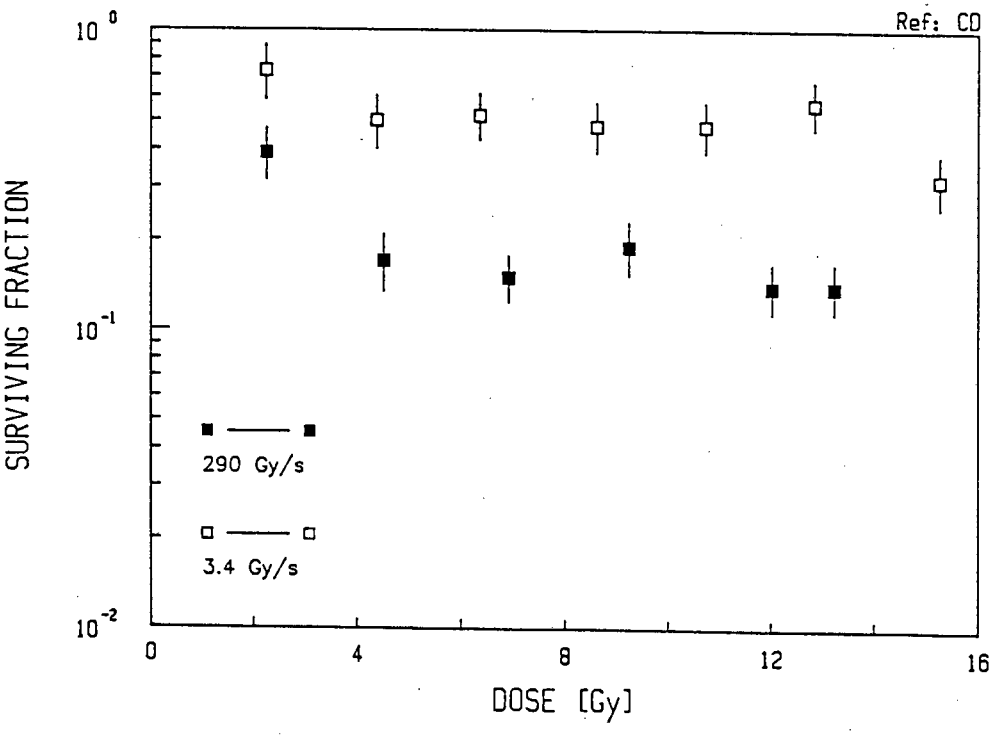

Figure 3.2 Survival data for V79 cells exposed to 3.6 MeV protons at high and low dose rate.

Two important questions arose from these results. Firstly, what was the cause of the constant level of survival? Secondly, was the difference between the high and low dose rate survival significant, or an experimental artifact?

A possible cause of the constant level of survival at high dose was that a fraction of the cells in the samples was not being exposed to the radiation. This could have occurred in three ways:

(1) The beam was missing a section of the cells as a result of poor alignment of the sample tubes. This was possible since the beam diameter was the same as the sample diameter.

(2) Close inspection of the irradiation vessels (figure 2.13, page 2-22) revealed an unacceptably large glue ridge. Cells were found to populate this ridge, which was thicker than 200 μm (the proton range), and were therefore protected from the radiation.

(3) The beam profile could have been non-uniform (it had not been measured at this stage), possibly resulting in some cells receiving very little radiation, and others receiving variable doses.

Attempts to correct factors (1) and (2) were made by constructing new irradiation vessels with a smaller sample diameter and a neater inner edge (see section 2.9 on page 2-28). The unusually high level of cell survival and the tendency for the surviving fraction to become constant at high dose persisted. An attempt to correct factor (3) was made by introducing a nickel scattering foil into the beamline (see section 2.1 on page 2-1 and 2.4 on page 2-15) and measuring the beam profile (see section 2.6, page 2-19), which was found to be somewhat non-uniform (see section 3.6).

The difference between the high and low dose rate survival was later found to be greatly reduced by using the more reliable aluminium Faraday cup for dosimetry (see section 2.3.1 on page 2-6).

After the new radiation vessels (see section 2.8, page 2-25) had been constructed, experimental work proceeded.

The survival of V79 cells in response to 3.6 MeV proton irradiation at a dose rate of 40 Gy/s (the accelerator maximum that day) is presented in figure 3.3. The survival curve appears to have a two-component slope similar to that of the high dose rate data in figure 3.1. Below a dose of about 6 Gy, the data appear to follow the familiar molecular model for cell survival (section 1.2.2.2, page 1-15), but at higher doses, they appear to follow the multi-target single-hit model (section 1.2.2.1, page 1-13) with a reduced slope. The solid

line represents a fit of the function:

$$f = e^{-(\alpha D+\beta D^2)}$$

to the first three data points (chisquared=0.61) and a fit of the function:

$$f = ne^{-\frac{D}{D_0}}$$

to the last four data points (chisquared=0.84), where f is the surviving fraction and D is the absorbed dose in Gy and the constants are determined by the fitting routines. Curve fitting at this stage has been carried out only to emphasise trends rather than to obtain meaningful numerical values. The broken line represents a linear fit to all the data points (chisquared=1.04). The chisquared values for the two component and single component fit suggest the validity of a two component fit.

This two component survival curve is reminiscent of the work of Epp et al. (1968) who found that the survival curves for bacteria, irradiated with ultra-high dose rate electron radiation, followed the usual survival curve initially, but at higher doses, showed a decrease in slope. They interpreted these results in terms of oxygen depletion as a result of the high dose rate irradiation (see figure 1.9, page 1-30). It was therefore decided to investigate a possible high dose rate effect on the intra-cellular oxygen of the V79 cells (see section 2.11, page 2-31).

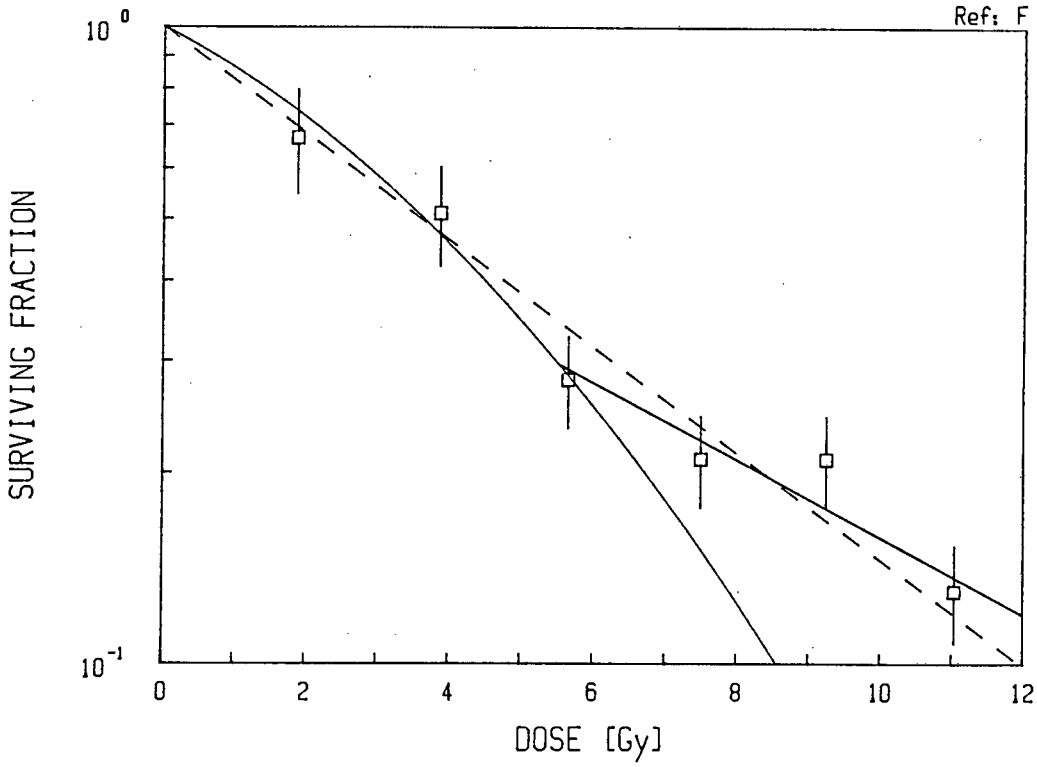

Figure 3.3 Survival curve for V79 cells exposed to 3.6 MeV protons at a dose rate of approximately 40 Gy/s. The solid lines represent the possible two components of the cell's response. The broken line represents a single component response function.

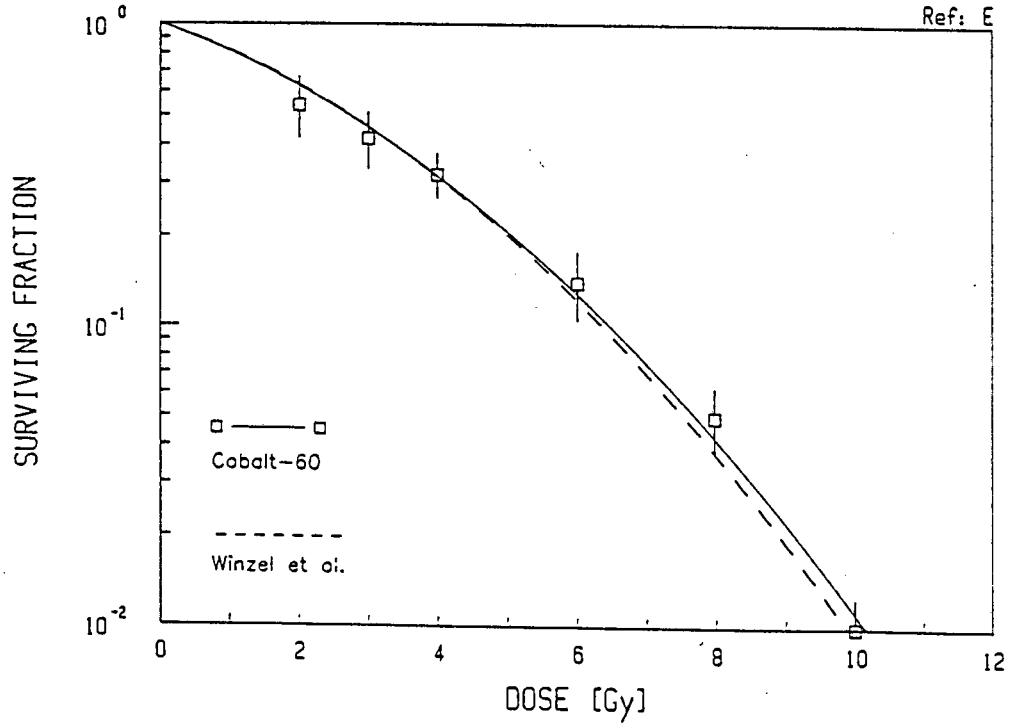

Figure 3.4 Survival curve for V79 cells exposed to cobalt-60 radiation at a maximum dose rate of 4.11 Gy/min (0.07 Gy/s).

3.2 THE COBALT-60 EXPERIMENT

The specially constructed radiation vessels used in this work needed to be tested in a standard cell colony assay to evaluate their suitability for such work. The survival of V79 cells irradiated in these vessels with cobalt-60 gamma radiation at a dose rate of 4.11 Gy/min is presented in figure 3.4. The survival data is well described by the molecular model for cell survival (section 1.2.2.2, page 1-15). The solid line represents a best fit of all the data points to the function:

$$f = e^{-(\alpha D+\beta D^2)}$$

where f is the surviving fraction and D is the dose in Gy. The fitting routine gives $\alpha = 0.18 \pm 0.01$ Gy^{-1} and $\beta = 0.027 \pm 0.002$ Gy^{-2}.

The results of Winzel et al. (1987) are presented for comparison ($\alpha = 0.17 \pm 0.02$ Gy^{-1}; $\beta = 0.031 \pm 0.007$ Gy^{-2}). These authors used the same V79 cell line, but irradiated the cells in suspension. Since there is good agreement between the two sets of measurements, it was concluded that the growth and irradiation of V79 cells in the special radiation vessels did not adversely affect the performance of the cell colony assay.

3.3 THE OXYGEN DEPLETION TEST

The results of V79 cells irradiated with 3.6 MeV protons at a dose rate of 80 Gy/s (the accelerator maximum that day), one set containing misonidazole, dissolved in MEM to a concentration of 4 mM, and one control set without misonidazole are presented in figure 3.5. At doses above 8 Gy the survival data are scattered and consequently no definite trend can be distinguished. The misonidazole samples also show this erratic behaviour at doses above 8 Gy and are not generally more sensitive to proton radiation than the control samples. The erratic behaviour above a dose of 8 Gy masked any possible oxygen depletion effect that might have existed. These inconclusive results probably reflect the uncertainty in the beam profile and the possiblity that a background of unirradiated cells still existed. This was possible since cells could populate the wall of the radiation vessel at a height above 200 μm (the proton range in water), thereby being protected from the proton radiation.

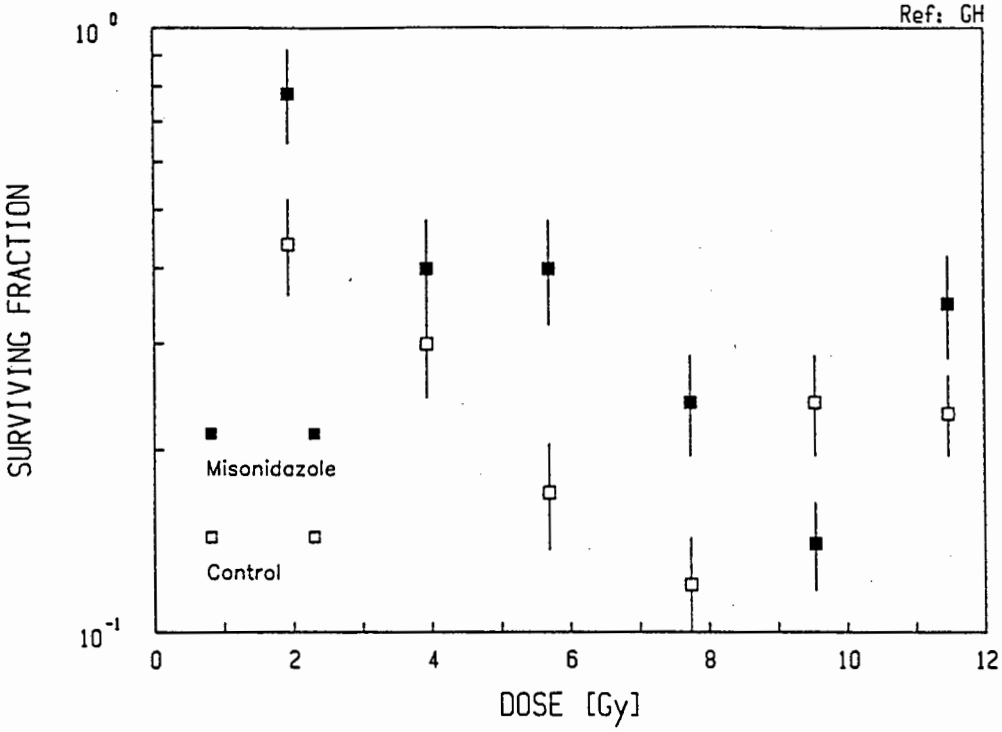

Figure 3.5 Survival data for V79 cells sensitised with 4 mM misonidazole and irradiated with 3.6 MeV protons at a dose rate of 80 Gy/s.

3.4 THE FARADAY CUPS

Table 3.1 contains the current measurements of the high and low current settings as measured by the internal and graphite Faraday cups as well as the PIXE count rates at these current settings (see section 2.3.1, page 2-6 and section 2.3.2, page 2-13). Errors reflect the standard deviation of 60 current measurements over one minute. It is clear that the high to low current ratio as measured by the internal Faraday cup falls within the uncertainty of the same ratio as measured by PIXE, while the graphite Faraday cup is completely unsatisfactory. The current as measured by the internal Faraday cup was therefore considered to be reliable. It is worth noting that

the high to low current ratio of 64.0 ± 0.9 is very much less than the expected value of 100 (see section 2.4, page 2-15). This discrepancy can be explained in terms of an unavoidable focus in the proton beam when striking the multiple scattering collimator (see section 2.1, page 2-1). This beam focus will therefore bias for proportionately higher currents in the smaller collimator and hence decrease the expected ratio, as observed.

Table 3.1: Calibration data for the graphite Faraday cup.

Device	Current		Ratio
	High	Low	
Graphite	2.39 ± 0.02 nA	0.15 ± 0.002 nA	16 ± 0.3
Internal	4.07 ± 0.04 nA	0.064 ± 0.0006 nA	64 ± 0.9
PIXE	85.0 ± 0.9 c/s	1.28 ± 0.08 c/s	66 ± 4

3.5 FILM CALIBRATION

The results of the Kodak X-Omat V film calibration with protons are presented in figure 3.6 (see section 2.6, page 2-19). The data are well fitted by a straight line with a correlation coefficient, R=0.997. Radiation dose is therefore proportional to the optical density of the film over a wide range of optical densities. Film density profiles will therefore be an accurate measure of the proton beam profiles.

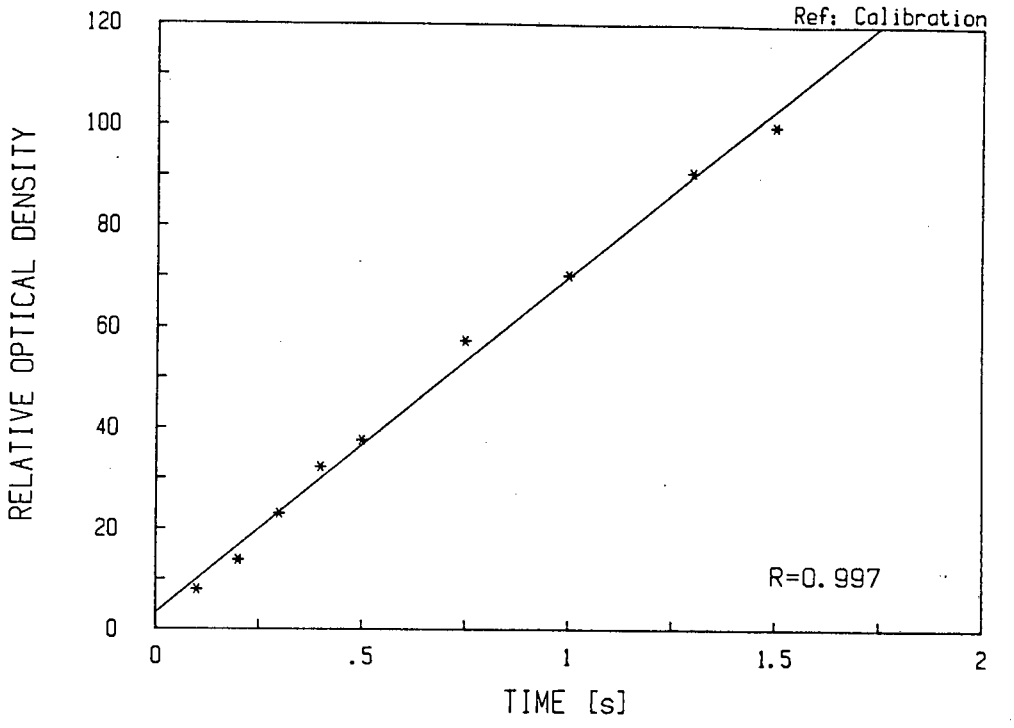

Figure 3.6 Kodak X-Omat V film calibration data and best fit straight line.

3.6 BEAM PROFILES

The results of scanning four proton irradiated films with a densitometer in two mutually perpendicular directions are presented in figure 3.7. By confining interest to the central 11 mm of the beam profiles (the diameter of the vessels), the edge effect, as a result of the densitometer detector having a diameter of 2 mm, is overcome. The radiation dose at the edge of the sample tube is frequently less than 0.5 of the central dose. The relatively poor quality of these beam profiles led to the nickel multiple scattering foil being moved to a distance of about 3 m from the beam window (see section 2.2, page 2-2).

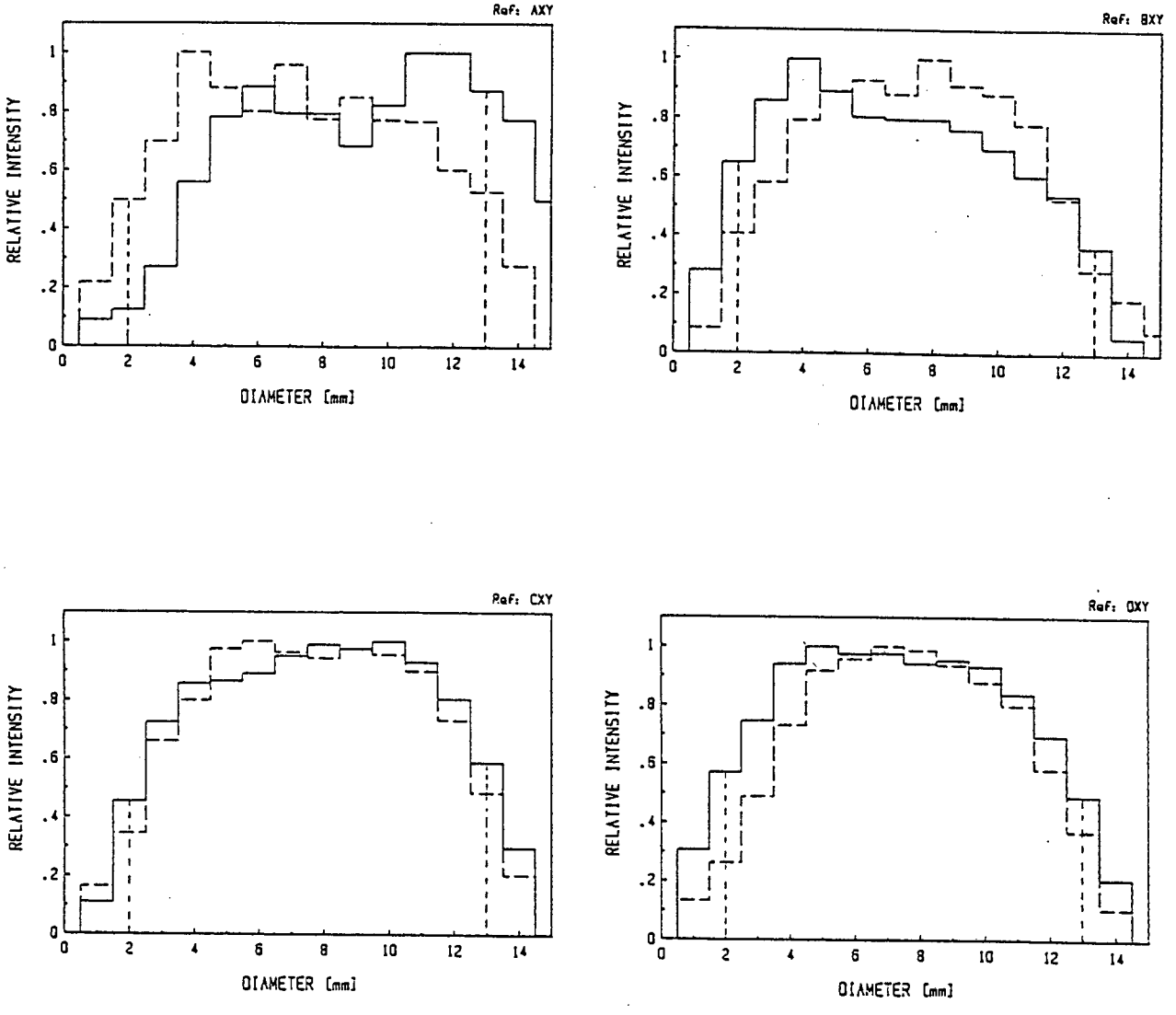

Figure 3.7 Typical beam profiles measured before the multiple scattering foil was appropriately moved. The vertical broken lines represent the edges of the irradiation vessels. Each profile represents the result of a densitometer scan of the film in two perpendicular directions, one direction is shown as a solid line, the other as a dashed line.

After the nickel scattering foil had been moved, the proton beam profile was measured again. Figures 3.8 and 3.9 show four measurements of the proton beam profile at high and low dose rate respectively. These profiles show a significant improvement on the earlier profiles in figure 3.7. They are more symmetrical and the radiation dose at the sample edge is generally higher, typically 0.6 of the central dose or higher. The high dose rate profiles in figure 3.8 compare well with the low dose rate profiles in figure 3.9, indicating that manipulating the current by altering the multiple scattering collimator aperture, as opposed to altering the beam focus, was effective in eliminating possible changes in the beam profile when the accelerator beam current was changed (see section 2.4, page 2-15).

Ideally, the beam profile should be very nearly uniform over the whole diameter of the irradiation vessel. In this respect, the beam profiles presented in figures 3.8 and 3.9 are still disappointing. These profiles reveal that the cells located at a radius greater than 4 mm from the centre of the irradiation vessel, could have received between 0.5 and 0.8 of the dose delivered to the central cells. These outer lying cells would have had a higher survival level than the central cells, thereby increasing the survival level of the whole sample to a value above what would normally be expected.

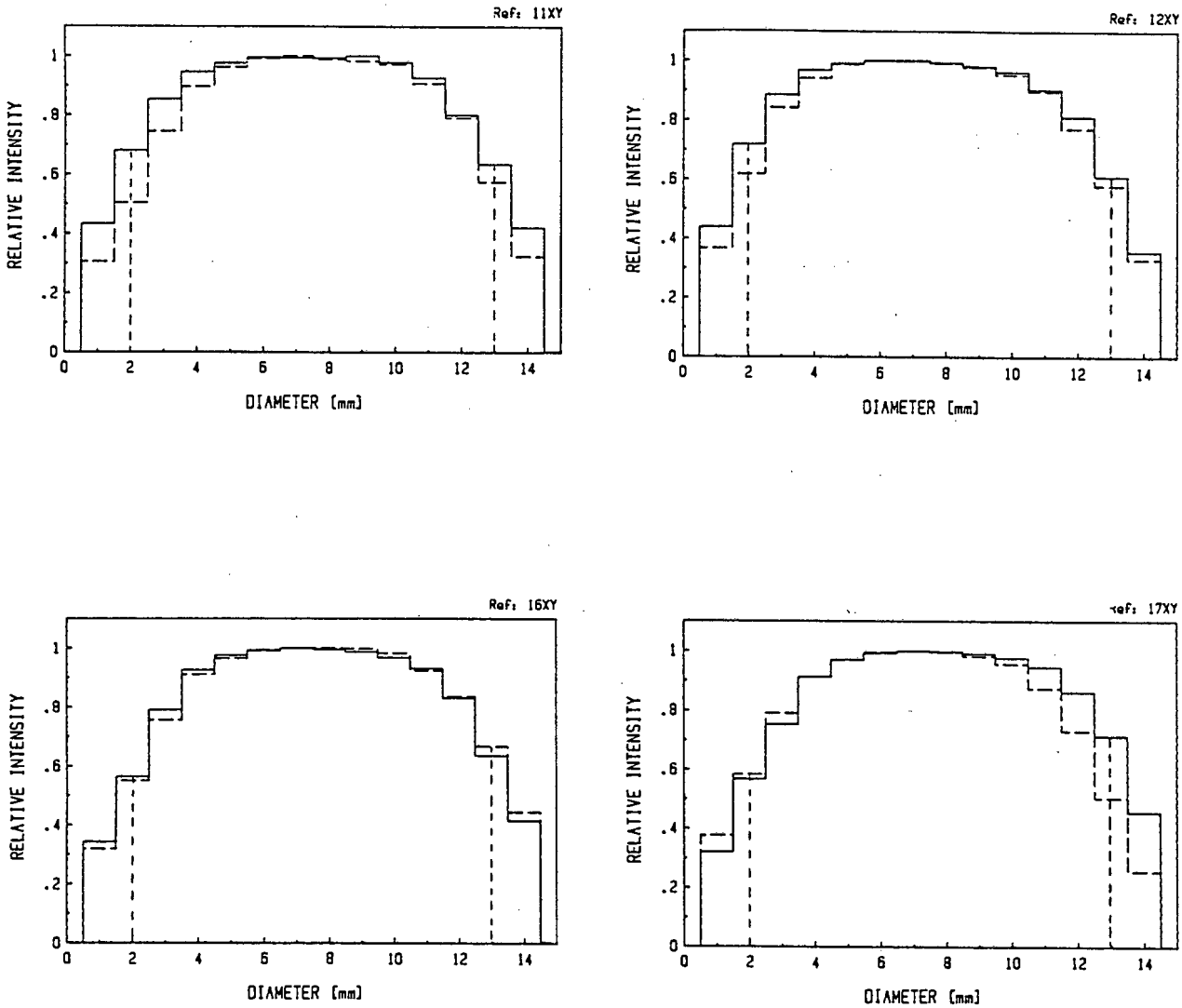

Figure 3.8 Beam profiles collected during the high dose rate irradiation presented in figure 3.10. Each profile shows the results of a densitometer scan of the film in two perpendicular directions, one direction is shown as a solid line, the other as a dashed line.

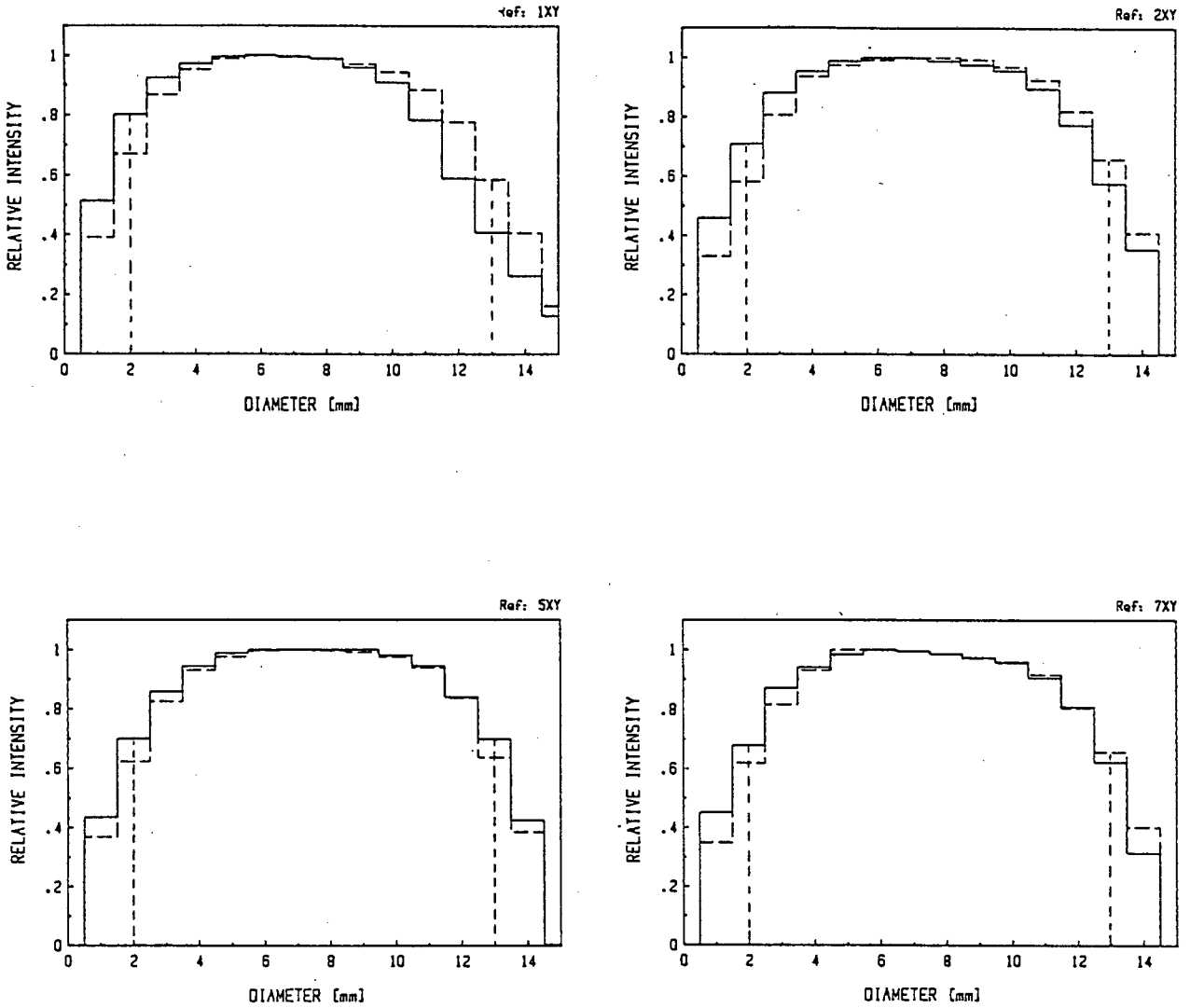

Figure 3.9 Beam profiles collected during the low dose rate irradiation presented in figure 3.10. Each profile shows the results of a densitometer scan of the film in two perpendicular directions, one direction is shown as a solid line, the other as a dashed line.

The beam profiles presented in figures 3.8 and 3.9 are probably the best that can be achieved with the present apparatus. The low dose intensity at the sample edge is probably due to the scattering of protons from the edges of the beam window and the beam defining aperture, G in the sample exposure apparatus (figure 2.13, page 2-22).

3.7 THE FINAL PROTON EXPERIMENT

The survival of V79 cells in response to 3.6 MeV proton irradiation at a dose rate of 240 Gy/s and 4.0 Gy/s is presented in figure 3.10. The proton beam profiles presented in figures 3.8 and 3.9 are the beam profiles measured during this experiment. The dose rates were calculated from the beam current as measured by the internal Faraday cup and checked by PIXE (see table 3.1).

The survival data presented in figure 3.10 continue to be unusually high, approaching a constant survival level of about 0.1 in the case of the low dose rate survival data. Figure 3.10 reveals no significant difference between survival of V79 cells exposed to 3.6 MeV protons at the dose rates investigated. The apparent difference between the earlier survival data (see figures 3.1 and 3.2) has been greatly reduced by the improved dosimetry used for this experiment. Although there is no significant difference between survival at the high and low dose rates investigated, qualitative differences are noticable. The low dose rate survival shows a

smooth fall in surviving fraction as the dose is increased up to a dose of about 12 Gy and then appears to remain constant at a level of about 0.1. The high dose rate survival shows a steeper fall up to a dose of about 5 Gy and thereafter appears to follow a more gentle fall as the dose is increased above this point. In this respect, the high dose rate data are similar to the results presented in figures 3.1 and 3.3 and show a similarity with the findings of Epp et al. (1968) presented in figure 1.9 (page 1-30). The low dose rate experiment presented in figure 3.10 is subject to the same experimental conditions as the high dose rate experiment, but does not appear to have the same two component slope as the high dose rate data, thereby supporting the possibility of a high dose rate effect on the intracellular oxygen, this possibility cannot be ignored since the result of the test for a dose rate effect on intracellular oxygen was inconclusive (see figure 3.5).

The high dose rate data could be influenced by three effects; a possible dose rate effect on intracellular oxygen as postulated by Epp et al. (1968), the beam profile and finally, the presence of a small background of unirradiated cells. The relative influence of these effects cannot be judged and need to be eliminated systematically through apparatus improvements.

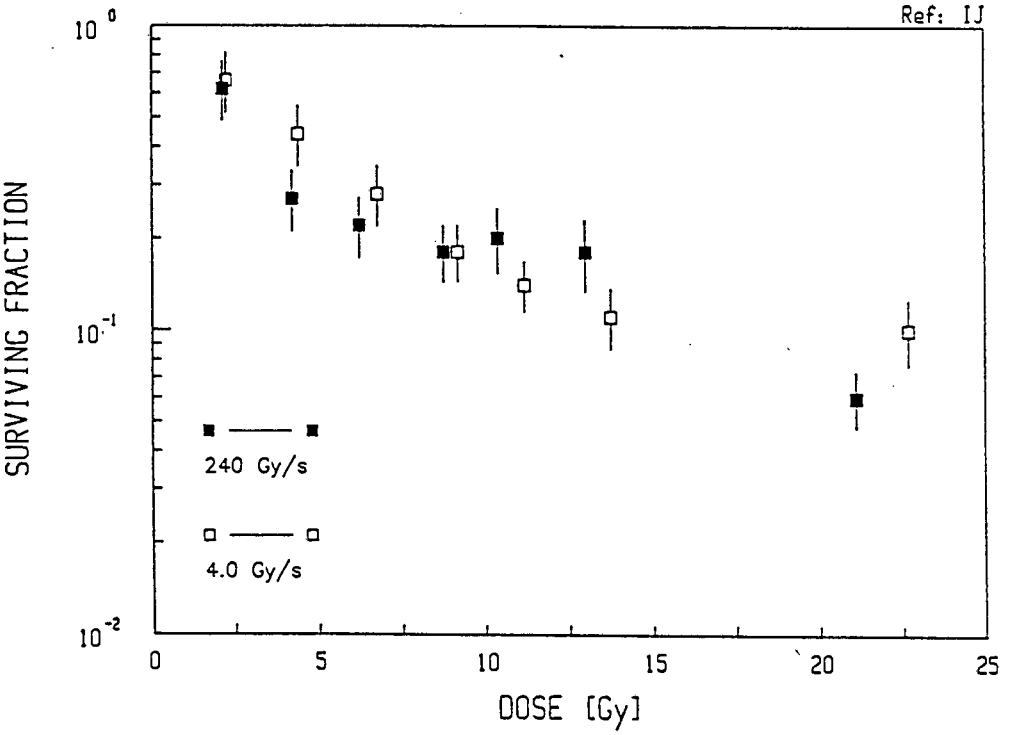

Figure 3.10 Survival data for V79 cells irradiated with 3.6 MeV protons.

3.7.1 CORRECTED SURVIVAL CURVES

Although the low dose rate results, presented in figure 3.10, show the surviving fraction tending towards a constant level of survival and hence appear to suggest a background of unirradiated cells, no attempt was made to correct for this because the limited data in the high dose region, made it impossible to reliably suggest a suitable background level for such a correction.

The effect of the beam profile has been assessed and details of the calculation of a dose correction factor are presented in

appendix D. Applying the dose correction factor (0.910) to the data in figure 3.10 yield the data in figure 3.11. The single high dose (>20Gy) points have been omitted because they suggest trends for which statistically insufficient data is recorded.

The molecular model for cell survival has been fitted to the corrected low dose rate data in figure 3.11 (α =0.196 $\pm$ 0.009; β = 0).

The curve for the results of the cobalt-60 irradiation from figure 3.4 is also drawn. This is useful since the RBE of low energy protons is expected to be greater than or equal to one and hence the proton irradiation data should lie on or below the cobalt-60 curve (Bird et al., 1980; Perris et al., 1986). This is clearly not the case in figure 3.11. The RBE of the low dose rate data in figure 3.11, relative to cobalt-60, measured at a surviving fraction of 0.1, is approximately 0.53 (6.5/12.2). The lack of a shoulder on the survival curve measured in this work and the fact that the RBE is less than one could be indicative of a dose rate effect. The dose rate of the low dose rate proton irradiation is 4 Gy/s while the dose rate of the cobalt-60 irradiation is only 0.07 Gy/s, which is more than 50 times smaller. The lack of a shoulder on the survival curve usually occurs with high LET radiations which have RBE values greater than one. The reversal of the usual trend in this case may therefore be significant although the possibility of a background of unirradiated cells renders the results inconclusive.

The corrected data of figure 3.11, like figure 3.10, suggests that there is no significant dose rate effect on V79 cell survival when irradiated at dose rates of 4 Gy/s and 240 Gy/s with 3.6 MeV protons. The qualitative differences in the high and low dose rate data are as for figure 3.10 (see earlier comments).

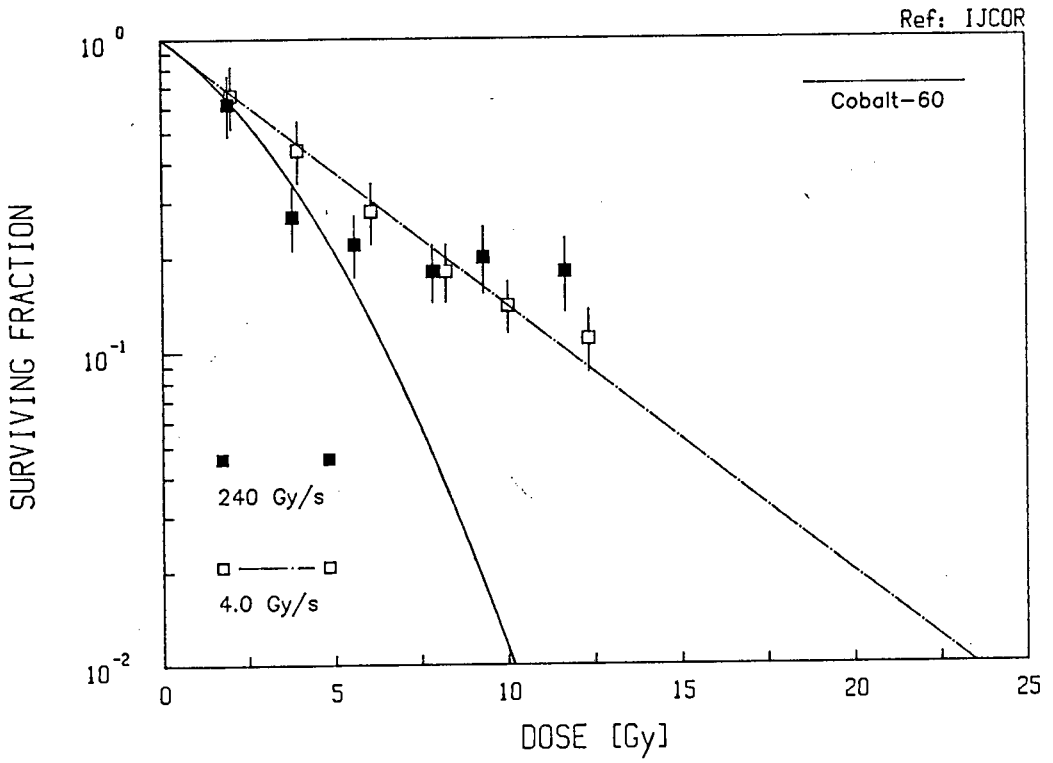

Figure 3.11 Survival data of figure 3.10 corrected for the effect of beam profile 17xy (figure 3.8). The molecular model has been fitted to the low dose rate data (α = 0.196 $\pm$ 0.009; β = 0). The function fitting the cobalt-60 data has been drawn for comparison.

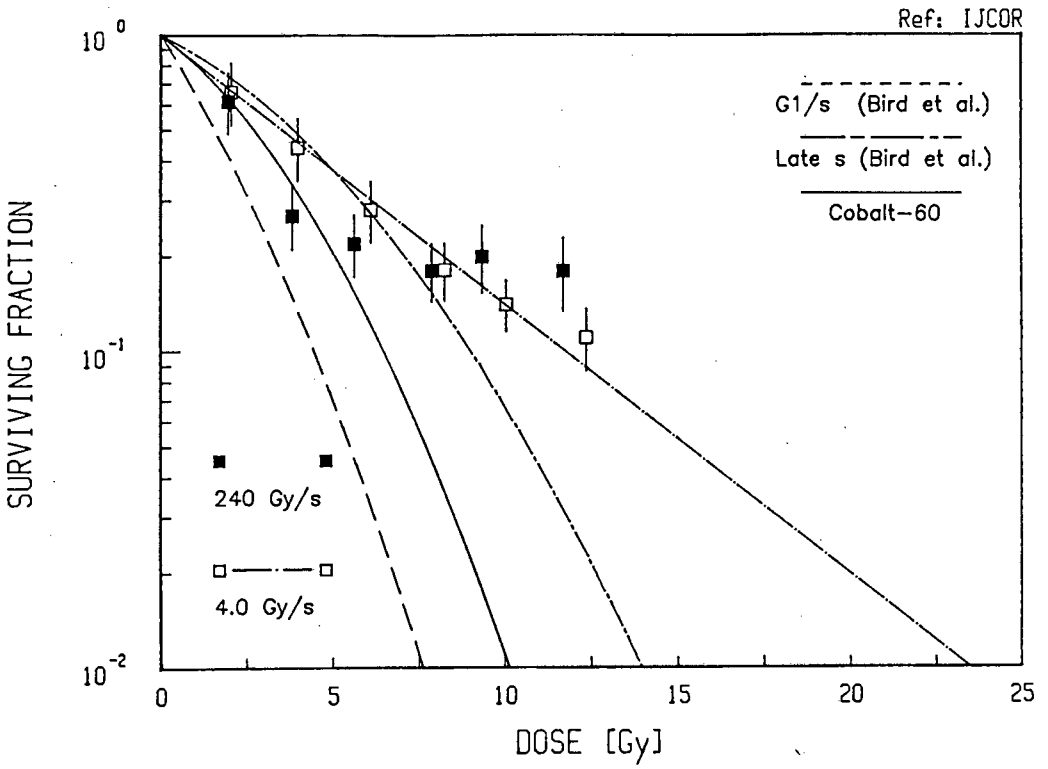

Figure 3.12 Corrected data from figure 3.11 compared with the work of Bird et al. (1980). The curve for the cobalt-60 data of figure 3.4 is also drawn.

The corrected results given in figure 3.11 are repeated in figure 3.12 together with the work of Bird et al. (1980) presented for comparison. Bird et al. (1980) measured survival curves for V79 cells synchronised at two stages of the cell cycle, the G_1/S transition and late S phase, which represent two extremes in radiosensitivity. Part of their work examined the survival curves of these cells irradiated with protons of LET similar to that used in this work (10 keV/μm). The parameters of their curves are presented in table 3.2.

Since this work used an unsynchronised population of cells, the

results are expected to lie between the curves from Bird et al. (1980). This is well approximated by the experimental data obtained in this work at doses below 6 Gy, while above 6 Gy, the experimental data deviates significantly from Bird et al. (1980).

While Bird et al. (1980) show that protons with an energy of 3.6 MeV have an RBE of 1.1, Perris et al. (1986) report an RBE of 1.95 for 3.0 MeV protons and 1.29 for 7.4 MeV protons and are therefore in disagreement with Bird et al. (1980) and the indications in this work. It is worth noting that the dose rate at which Bird et al. (1980) performed their proton irradiation was less than 1 Gy/s, while Perris et al. (1986) used a dose rate less than 0.1 Gy/s. Table 3.3 summarises the dose rates used by Perris et al. (1986), Bird et al. (1980) and this work, both for the proton radiation and the photon radiation (cobalt-60 and 250 kV X-rays). The results of this work may therefore be affected by the significantly different dose rate at which the proton radiation was performed.

Table 3.2: Parameters of fitting functions.

	Alpha Gy^{-1}	Beta Gy^{-2}	
Low dose rate	0.196 ± 0.009	-	
G_1/S (Bird et al.)	0.399 ± 0.069	0.027 ± 0.011	*
Late S (Bird et al.)	0.122 ± 0.018	0.0149 ± 0.0016	*
cobalt-60	0.18 ± 0.01	0.027 ± 0.002	

* From Bird et al. (1980), see text.

Table 3.3 Table summarising the dose rates used by the different authors.

	Proton Gy/s	Photon Gy/s
Perris et al. (1986)	0.09	0.11
Bird et al. (1980)	< 1	< 1
This Work	4 - 300	0.07

4 CHAPTER FOUR: CONCLUSIONS

A number of experimental techniques have been developed and tested:

(1) General cell handling procedures were perfected. V79 cells attached to Mylar and formed a monolayer as in normal tissue culture flasks. The cells were unaffected by the fixative used in the construction of the special radiation vessels and the sterilisation of these vessels was found to be adequate.

(2) Dosimetry for the irradiation of monolayers of V79 cells was fairly straight forward since the proton energy was nearly constant as the protons passed through the thin (6 μm) layer of cells. The LET was therefore constant and the dose rate was therefore proportional to the proton beam current. This current can, in principle, be accurately measured with a suitably constructed Faraday cup.

(3) Kodak X-Omat V film was used for measuring proton beam profiles, while multiple scattering in thin metal foils was used to create more homogeneous beam profiles.

(4) Particle induced x-ray emission (PIXE) was used to confirm the ratio of the high to low current measurements.

It is difficult to draw any definite conclusion regarding a possible dose rate effect on cell survival of 3.6 MeV proton irradiation at dose rates of 240 Gy/s and 4 Gy/s, because the following possible experimental artifacts were present simultaneously:

(1) A possible background of unirradiated cells could have been present. Cells which attach to the walls of the irradiation vessel at a distance of more than 200 μm from the vessel base would be protected from the proton radiation because of the limited proton range.

(2) The above influence made the evaluation of a possible dose rate effect on intracellular oxygen impossible to assess. Such an effect may well be present and could account for the qualitative difference in the survival curve shapes of the high and low dose rate irradiation.

Subject to these reservations, the experimental data (figure 3.10, page 3-18) do not show any significant effect on the survival level of V79 cells irradiated at 240 Gy/s or 4 Gy/s.

The data presented in figure 3.11 (page 3-20) seem to suggest a possible dose rate effect between irradiation at normal dose rates (about 0.07 Gy/s) and the high and very high dose rates used in this work (4 Gy/s and 240 Gy/s). However, before such a statement can be made with any certainty, the above influences would need to be eradicated through the following apparatus refinements:

(1) The use of a larger proton field to overcome the problem of poor beam profiles at the sample edges, probably caused by scattering from the edges of the beam window and beam defining apertures.

(2) The use of irradiation vessels with a larger diameter which could allow for the cells to be preferentially plated in the centre of the irradiation vessel and thereby prevent the problem of cells attaching to the vessel wall out of range of the protons.

(3) The use of a large spherical scattering chamber, with a central multiple scattering foil, to create an adequate proton beam for the irradiation of monolayer cellular samples, as recently suggested by Perris et al. (1986), has a number of advantages:

(3.1) The possibility of multiple scattering from the beam line and the generation of a lower energy proton component is eliminated by this design.

(3.2) This irradiation arrangement allows for monitoring the beam current while the cells are being irradiated.

(3.3) The Perris et al. (1986) arrangement also allows for irradiation of cells at much lower dose rates and eliminates the problem of measuring beam currents which are too low for standard current integrators. By exploiting the strong angular dependence of the multiple scattered beam, cell irradiation could take place at a current 100 times lower than measured by the Faraday cup. This is desirable for comparison with survival curves obtained with standard radiation types at conventional dose rates. The problem of a strong dependence of the beam profile on the scattering angle is minimised by irradiating the samples in two steps, after half the dose has been delivered to the cells, the vessel is rotated 180° and the second half of the dose is delivered (Perris et al., 1986).

With the above improvements to the apparatus, the question of a dose rate effect on cell survival could be re-investigated. The influence of high dose rate irradiation on intracellular oxygen could also be analysed. This information would be valuable if very high dose rates are ever envisaged for proton radiotherapy.

In general, all the experimental techniques which have been perfected could be used, in a modified experimental arrangement, to undertake further biological experiments with low energy proton beams.

APPENDIX A - GROWTH CURVE

A stock culture flask (T-75) of V79 cells was harvested with trypsin (0.5% in .1 ml) and the cell concentration was determined with the aid of a haemocytometer. The cell suspension was diluted until a concentration of about 4.5×10^4 cells/ml was achieved. One millilitre of this solution was placed into 8 sets of 3 tissue culture flasks (T-25). The growth medium, Ham's Minimum Essential Medium (MEM), supplemented with 10% foetal calf serum and antibiotics: Penicillin (100 u/ml), Streptomycin (100 µg/ml) and Tylocin (0.5%), was added to each flask. The flasks were incubated at 37 °C in a humidified 5% CO_2, 95% air atmosphere. The total cell number in 3 flasks was determined, with the aid of a haemocytometer, at various times over a period of 120 hours, until all 8 sets of 3 flasks had been used. The average number of cells in each flask was divided by the base area of the flask to yield the number of cells/cm^2.

The results are shown in figure A.1. After an initial lag, which was partly a result of cell mortality in handling and partly a delay in the cell cycle while the cells attached to the flask base, the cells began to grow exponentially until a concentration of about 5×10^5 cells/cm^2 (achieved after about 70 hours). At this concentration, contact inhibition caused the cells to cease dividing and the cell concentration remained fairly constant for the next 50 hours.

A linear fit to the exponential region of the curve gave the slope = 0.0955 and the intercept = 6.481 with the correlation coefficient R = 0.99996.

The number of cells N followed the following equation:

$$N = 652.6\, e^{0.0955\, t} \qquad (A.1)$$

where t was the time in hours.

From this equation, we found that the doubling time for the V79 cells, under the culture conditions described, was 7.3 hours.

Since the area of the 11 mm diameter radiation vessels used in this work was 0.95 cm^2, it follows that a maximum of 5 x 10^5 cells represented confluency in these vessels.

In the radiation experiments in this work, the cells were placed in the radiation vessels about 24 hours before they were irradiated. The number of cells chosen to be placed in the radiation vessels was 5 x 10^4. After an initial lag of about 12 hours (see figure A.1) these cells would then grow exponentially for 12 hours before being irradiated. From equation A.1, the number of cells in each vessel would be about 1.6 x 10^5. This means that the cells were almost 2 generations from the maximum and were therefore irradiated while in exponential growth phase.

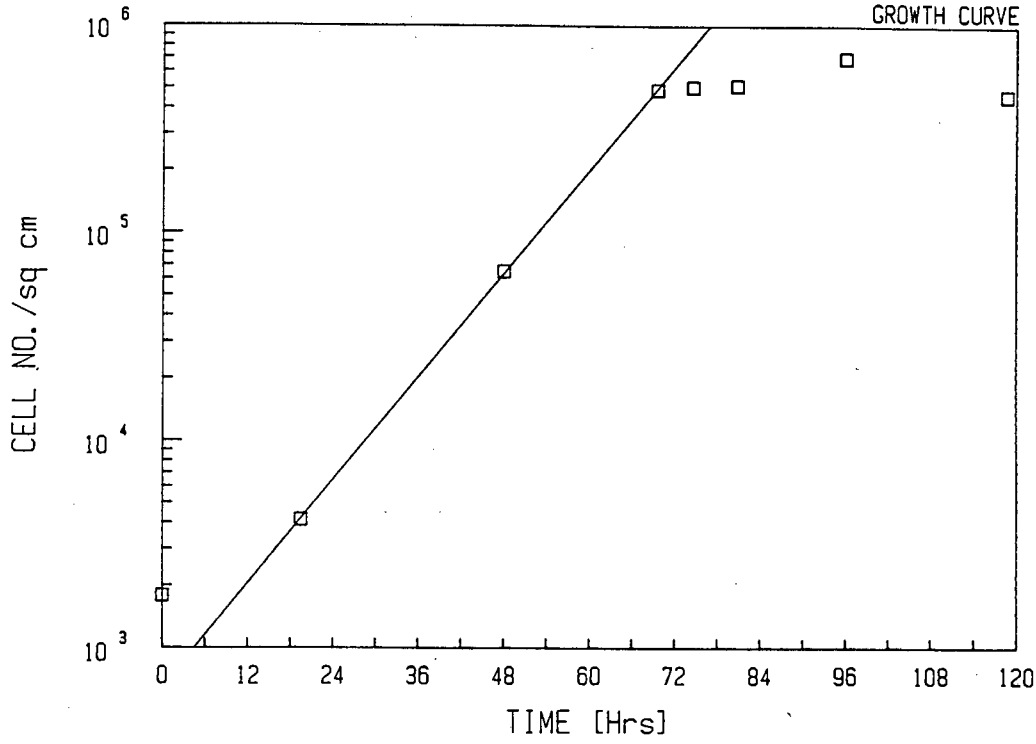

Figure A.1 Growth curve for V79 cells cultured as described in this work.

APPENDIX B - ENERGY LOSS IN HAVAR

The energy loss of 4.25 MeV protons in Havar was calculated by performing a weighted sum of the energy losses of the protons in each element (Janni, 1982). The calculation is summarised in table B.1. The symbol, a, is used to denote the percentage weight contribution of each element to the Havar foil.

Table B.1 The energy losses of 4.25 MeV protons in various elements.

	a%	Eloss MeV/cm	axEloss/100 MeV/cm
Be	0.04	138	0.0552 ± 0.0002
C	0.2	193	0.39 ± 0.01
Cr	20.0	365	73.0 ± 0.9
Mn	1.6	389	6.22 ± 0.05
Fe	17.46	417	72.8 ± 0.9
Co	42.5	455	193 ± 2
Ni	13.0	471	61.2 ± 0.6
Mo	2.4	434	10.4 ± 0.4
W	2.8	618	17.3 ± 0.7
		Total	435 ± 3

The energy loss of 4.25 MeV protons in 6.35 μm Havar was therefore 276 ± 2 kev.

APPENDIX C - MULTIPLE SCATTERING

4.5 MeV Protons incident on 6.35 μm Ni foil

$$\beta^2 = 1 - \left(1 + \frac{E}{MC^2}\right)^{-2} = 0.00953$$

$$(pv)^2 = (E^2 + 2EMc^2)\cdot\beta^2 = 80.645$$

$$\chi_c^2 = 0.1569\ \{Z(Z+1)z^2/A\}\{t/(pv)^2\}$$

where Z = atomic number of scattering foil

z = atomic number of incident particle

t = thickness of foil (g/cm^2)

A = atomic weight of foil material

pv = momentum × velocity of incident particle (MeV)

$\beta = \frac{v}{c}$

χ_c = that angle for which, on average, there is only one collision with $\chi > \chi_c$ as the particle traverses the foil.

$\therefore\ \chi_c^2 = 1.524 \times 10^{-4}$

$\therefore\ \chi_c = 0.0123$

$$b = \ell n\ [2730\{(Z+1)Z^{1/3}z^2t/(A\beta^2)\}] - 0.1544$$

$\therefore\ b = 7.643$

$\therefore\ B \approx 9.9$

$\therefore\ B^{\frac{1}{2}} \approx 3.15$

$\therefore\ x_w \approx 0.934$

(Marion and Zimmerman, 1967)

$$F_G(x) = \exp - \left(\frac{x^2}{x_w^2}\right)$$

For 99% intensity, $\exp - \left(\frac{x^2}{x_w^2}\right) = 0.99$

$$\therefore \quad -\frac{x^2}{x_w^2} = \ln 0.99$$

$$\therefore \quad x = 0.0934$$

$$x = \frac{\theta}{\chi_c} B^{\frac{1}{2}}$$

$$\therefore \quad \theta_{99} = 0.0934 \times 0.0123 \times 3.15 = 3.619 \times 10^{-3} \text{ rad}$$

$$\therefore \quad \theta_{99} = 0.21°$$

For a 2 cm sample diameter, the distance from the foil to the beam window must be 273 cm.

APPENDIX D - BEAM PROFILE EFFECT ON SURVIVAL

The beam area was divided up into 1 mm rings as shown in figure D.1 (r = 0.5, 1.5, 2.5, 3.5, 4.5, 5.5 mm). Since the beam profiles shown in figures 3.8 and 3.9 are very similar, one typical profile was chosen and used to correct the experimental data. Beam profile 17xy was chosen (figure 3.8). The profile was applied over the radius (r) shown in figure D.1. There were two measures of the beam profile, x and y, and each of these contributes two measures of the profile over the radius (r), one in each direction from the central point. The four measures of the beam profile were averaged (see table D.1) and the average profile was applied over the radius (r).

Table D.1 The beam profile fractions, normalised to one at the maximum.

Ring No.	Prof. 1	Prof. 2	Prof. 3	Prof. 4	Ave.
1 (r=0.5)	1.00	1.00	1.00	1.00	1.00
2 (r=1.5)	0.991	0.982	0.996	0.993	0.991
3 (r=2.5)	0.976	0.956	0.970	0.971	0.968
4 (r=3.5)	0.945	0.873	0.913	0.912	0.911
5 (r=4.5)	0.861	0.731	0.791	0.754	0.784
6 (r=5.5)	0.714	0.504	0.584	0.567	0.592

The average profile is shown in figure D.2 as a solid line. The area under the average profile is 4.746 (arbitrary units), the uniform profile drawn as a dotted line is therefore drawn at a height of 0.863 on the relative intensity axis. The area of each ring and the fraction of the total area was computed and is shown in table D.2.

Table D.2 The beam profile radius and ring area analysis.

Ring No.	Area (mm)	Fraction
1 (r=0.5)	0.785	0.0083
2 (r=1.5)	6.283	0.0661
3 (r=2.5)	12.566	0.132
4 (r=3.5)	18.850	0.198
5 (r=4.5)	25.133	0.264
6 (r=5.5)	31.416	0.331
Total	95.033	0.9994

The average profile relative intensity divided by the uniform profile relative intensity gives a dose factor for each ring in figure D.1. The dose factor multiplied by the area fraction gives a dose correction factor for each ring. These correction factors are summed to give an overall dose correction factor. These calculations are shown in table D.3.

Table D.3 Data to calculate the overall dose correction factor.

Ring No.	Ave. Profile	Uniform Profile	Dose Factor	Area Fraction	DfxAf
1 (r=0.5)	1.00	0.863	1.159	0.0083	0.0096
2 (r=1.5)	0.991	0.863	1.148	0.0661	0.076
3 (r=2.5)	0.968	0.863	1.122	0.132	0.148
4 (r=3.5)	0.911	0.863	1.056	0.198	0.209
5 (r=4.5)	0.784	0.863	0.908	0.264	0.240
6 (r=5.5)	0.592	0.863	0.686	0.331	0.227
				Total	0.910

The overall dose correction factor is 0.910. The effect of this dose correction factor applied to the raw data of figure 3.10 (page 3-18) is shown in figure D.3.

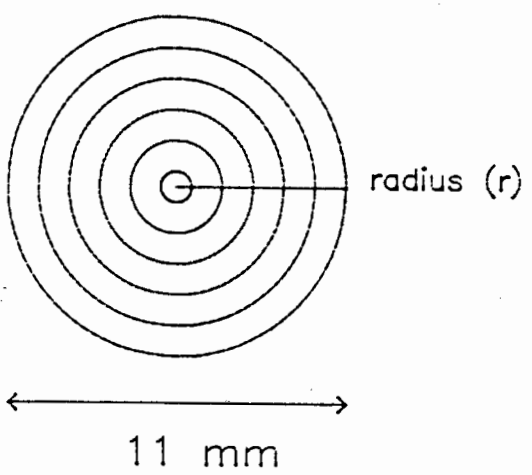

Figure D.1 The area of the sample vessel, divided up in rings. This is done so that the beam profile may be applied to the vessel area.

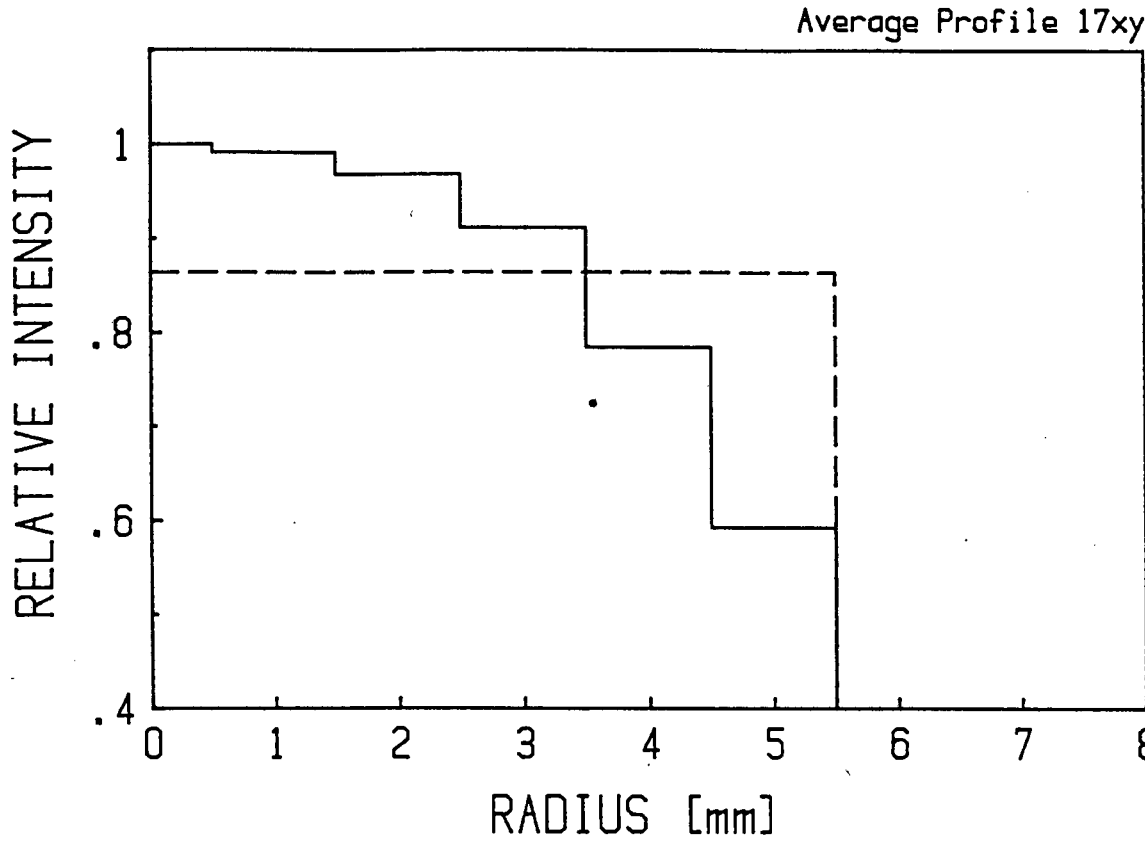

Figure D.2 The average beam profile for profile 17xy (figure 3.8), shown as the solid line. The dotted line represents the equivalent uniform beam profile.

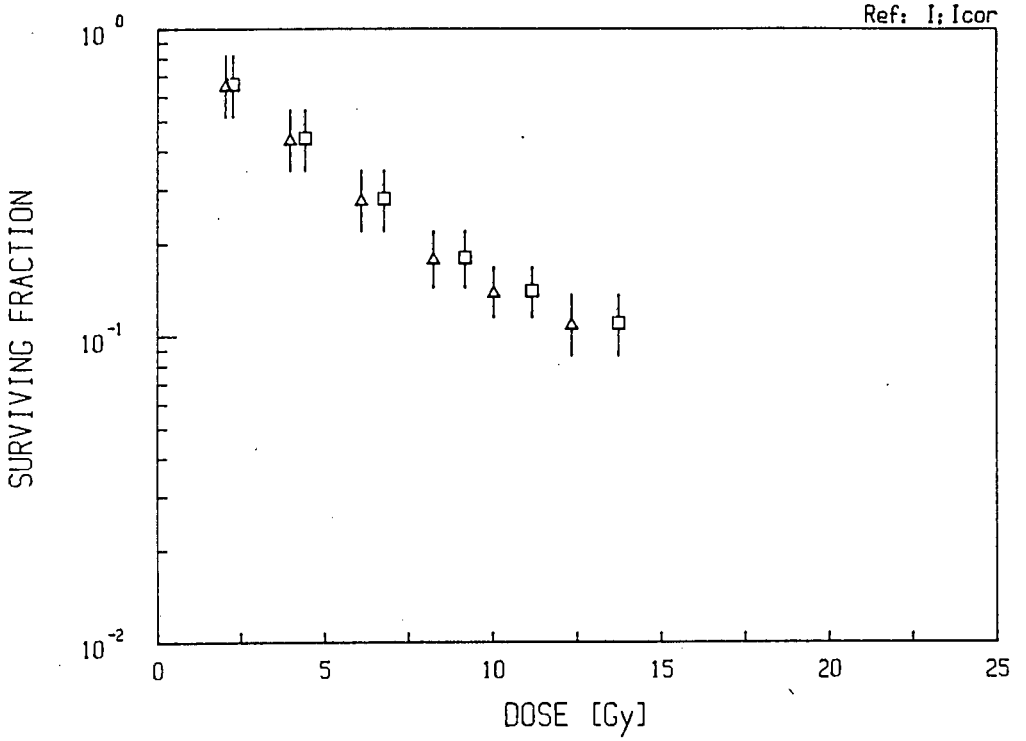

Figure D.3 The effect of the beam profile correction on the raw data, shown as squares, of figure 3.10 (page 3-18). The corrected data, shown as triangles, is seen to lie at slightly lower doses, thereby increasing the RBE.

APPENDIX E - RUTHERFORD BACKSCATTERING

$$A = \int_{\Omega} \left(\frac{d\sigma}{dr}\right) d\Omega \cdot Q \cdot Nt$$

where A is the number of particles detected

Q is the total number of incident particles

Nt is the number of target atoms per unit area.

$$\frac{d\sigma}{d\Omega} = \left(\frac{Z_1 Z_2 q}{16\pi\varepsilon_0 E}\right)^2 \frac{4}{\sin^4\theta} \frac{\left\{\left[1-\left(\left(\frac{m_1}{m_2}\right)\sin\theta\right)^2\right]^{\frac{1}{2}} + \cos\theta\right\}^2}{\left[1-\left(\left(\frac{m_1}{m_2}\right)\sin\theta\right)^2\right]^{\frac{1}{2}}}$$

where m_1 is the mass of the incident particle

m_2 is the mass of the target atom

Z_1 is the atomic number of the incident particle

Z_2 is the atomic number of the target nucleus

E is the energy of the incident particle in eV

q is the electronic charge.

The incident particle will not be backscattered after it has penetrated half its range. At half the range the particle's energy will be greater than $\frac{1}{2}E_0$. For an approximation the energy can be taken as $\frac{1}{2}E_0$. The average energy of particle useful for substitution into the constant above is given by

$$\left(\frac{I}{E}\right)^2 = \frac{1}{1.8}\int_{1.8}^{3.6} \frac{1}{E^2}\cdot dE = 2.55 \text{ MeV}$$

$$\therefore \quad \left(\frac{Z_1 Z_2 q}{16\pi\varepsilon_0 E}\right)^2 \approx 0.007173 \text{ b}$$

$$\int_{\Omega} \frac{d\sigma}{d\Omega} \cdot d\Omega = \int_{0}^{2\pi} \int_{\frac{3}{4}\pi}^{\pi} \frac{d\sigma}{d\Omega} \sin\theta \, d\theta \, d\phi$$

$$\therefore \quad \int_{\Omega} \frac{d\sigma}{d\Omega} \cdot d\Omega = 2\pi \left(\frac{Z_1 Z_2 q}{16\pi\varepsilon_0 E} \right)^2 \int_{\frac{3}{4}\pi}^{\pi} \frac{4\sin\theta}{\sin^4\theta} \frac{\left\{ \left[1 - \left(\left(\frac{m_1}{m_2} \right) \sin\theta \right)^2 \right]^{\frac{1}{2}} + \cos\theta \right\}^2}{\left[1 - \left(\left(\frac{m_1}{m_2} \right) \sin\theta \right)^2 \right]^{\frac{1}{2}}} d\theta$$

The integration limits are for a worst case geometry, where the Faraday cup is the graphite cup with a solid angle for proton backscatter of 1.84 steradians. This represents the largest possible backscatter solid angle.

$$\int_{\Omega} \frac{d\sigma}{d\Omega} \cdot d\Omega = 1.528 \times 10^{-2} \ \frac{b}{sr}$$

$$\therefore \quad A = 1.528 \times 10^{-2} \times 10^{-24} \times 5.02 \times 10^{20} \times Q$$

$$= 7.67 \times 10^{-6} \ Q$$

taking t as 0.005 cm, which is half the range of 3.6 MeV proton in graphite (Janni, 1982).

$\therefore$ 1 in 100 000 protons will be backscattered out of the graphite Faraday cup,

i.e. 0.001%.

REFERENCES

Ainsworth E.J., Leong G.F., Kendall K., Alpen E.L. and Allbright M.L. (1964), In Hall E.J., Brit. J. Radiol. 45 (1972) 81

Alper T., Gillies N.E. and Elkind M.M., Nature 186 (1960) 1062

Alper T., Cellular Radiobiology, Cambridge University Press (1979)

Andrews H.L., Radiation Biophysics, Prentice Hall (1961)

Archambeau J.O., Bennett G.W. Levine G.S., Cowen R. and Akanuma A., Radiology 110 (1974) 445

Barendsen G.W., Beusker T.L.J., Vergroesen A.J. and Budke L., Rad. Res. 13 (1960) 841

Bedford J.S. and Mitchell J.B., Rad. Res. 54 (1973) 316

Bethe H.A., Ann. Physik. 5 (1930) 325

Bettega D., Birattari C., Bombana M., Conti A.M.F., Gallini E., Pelucchi T. and Lombardi L.T., Rad. Res. 77 (1979) 85

Bird R.P., Rohrig N., Colvett R.D., Geard C.R. and Marino S.A., Rad. Res. 82 (1980) 277

Bragg W.H. and Kleeman R., Phil. Mag. 8 (1904) 726

Brustad T., Adv. Biol. Med. Phys. 8 (1962) 161

Chadwick K.H. and Leenhouts H.P., Phys. Med. Biol. 18 (1973a) 78

Chadwick K.H. and Leenhouts H.P., Euratom Report EUR 4918 (1973b). In Chadwick K.H. and Leenhouts H.P., The Molecular Theory of Radiation Biology, Springer-Verlag (1981)

Coggle J.E., Biological Effects of Radiation, Taylor and Francis Ltd (London) (1983)

Denekamp J. and Fowler J.F. (1966), In Hall E.J., Brit. J. Radiol. 45 (1972) 81

Dewey D.L. and Boag J.W., Nature 183 (1959)

Elkind M.M. and Whitmore G.F., The Radiobiology of Cultured Mammalian Cells, Gordon and Breach, New York (1967)

England J.B.A., Techniques in Nuclear Structure Physics (part

1), Macmillan Press Ltd (1974)

Epp E.R., Weiss H. and Santomasso A., Rad. Res. 34 (1968) 320

Fitzgerald J.J., Brownell G.L. and Mahoney F.J., Mathematical Theory of Radiation Dosimetry, Gordon and Breach (1967)

Fu K., Phillips T.L., Kane L.J. and Smith V., Radiology 114 (1975) 709

Goitein M., Suit H.D., Gragoudas E., Koehler A.M. and Wilson R., Rad. Res. Sup. 104 (1985) S-297

Griem M.L., Skaggs L.S., Lanzl L.H. and Malkinson F.D., Annals of The New York Academy of Medicine 161 (1969) 317

Hall E.J. and Bedford J.S., Rad. Res. 22 (1964) 305

Hall E.J., Brit. J. Radiol. 45 (1972) 81

Hall E.J., Radiobiology for the Radiobiologist, Harper and Row (1978) 2nd edition

Hall E.J., Kellerer A.M., Rossi H.H. and Lam Y-M.P., Int. J. Rad. Onc. Biol. Phys. 4 (1978) 1009

Hall E.J., Brit. J. Radiol. 54 (1981) 773

Hornsey S. and Alper T., Nature 210 (1966) 212

Hornsey S., Brit. J. Radiol. 43 (1970) 802

Hornsey S. and Bewley D.K., Int. J. Radiat. Biol. 19 (1971) S 479

Hospital Physicists Association, Phys. in Med. and Biol. 28 (1983) 1097

ICRU, Report 35 (1984)

Janni J.F., Atomic Data and Nuclear Data Tables 27 (1982) 147

Kellerer A.M. and Rossi H.H., Curr. Topics Radiat. Res. 8 (1972) 85

Kellerer A.M. and Chemelevsky D., Rad. Res. 63 (1975) 226

Koehler A.M. and Preston W.M., Radiology 104 (1972) 191

Larsson B., Brit. J. Radiol. 34 (1961) 143

Larsson B. and Sarby B., (1975) In Raju M.R., Heavy Particle Radiotherapy, Academic Press (1980)

Lindop P. and Rotblat J., (1963) In Hall E.J., Brit. J. Radiol. 45 (1972) 81

Marion J.B. and Zimmerman B.A., Nucl. Instrum. Methods 51 (1967) 93

Matteson S. and Nicolet M.A., Nucl. Instrum. Methods 160 (1979) 301

Michaels H.B., Ling C.C., Epp E.R. and Peterson E.C., Rad. Res. 85 (1981) 567

Michaels H.B., Int. J. Rad. Onc. Biol. Phys. 8 (1982) 427

Mitchell J.B., Bedford J.S. and Bailey S.M., Rad. Res. 79 (1979a) 537

Mitchell J.B., Bedford J.S. and Bailey S.M., Rad. Res. 79 (1979b) 520

Mitchell J.B., Bedford J.S. and Bailey S.M., Rad. Res. 79 (1979c) 552

Peisach M., Private Comm., NAC, 1988

Perkins D.H., Introduction to High Energy Physics, Addison-Wesley (1982)

Perris A., Pialoglou P., Katsanos A.A. and Sideris E.G., Int. J. Radiat. Biol. 50 (1986) 1093

Puck T.T. and Marcus P.I., J. Exp. Med. 103 (1956) 653

Raju M.R., Heavy Particle Radiotherapy, Academic Press (1980)

Robertson J.B., Williams J.R., Schmidt R.A., Little J.B., Flynn D.F. and Suit H.D., Cancer 35 (1975)

Suit H.D., Goitein M., Tepper J., Koehler A.M., Schmidt R.A. and Schneider R., Cancer 35 (1975) 1646

Suit H.D., Goitein M., Tepper J.E., Verhey L., Koehler A.M., Schneider R. and Gragoudas E., Int. J. Rad. Onc. Biol. Phys. 3 (1977) 115

Tepper J., Verhey L., Goitein M., Suit H.D. and Koehler A.M., Int. J. Radiat. Onc. Biol. Phys. 2 (1977) 1115

Tobias C.A., Van Dyke D.C., Simpson M.E., Anger H.O., Huff R.L. and Koneff A.A., Am. J. Roentgenol. Radiat. Ther. Nucl. Med. 72 (1954) 1

Urano M., Goitein M., Verhey L., Mendiondo O., Suit H.P. and

Koehler A., Int. J. Rad. Onc. Biol. Phys. 6 (1980) 1187

Urano M., Verhey L.J., Goitein M., Tepper J.E., Suit H.D., Mendiondo O., Gragoudas E.S. and Koehler A., Int. J. Rad. Onc. Biol. Phys. 10 (1984) 509

Verhey L.J., Koehler A.M., Mc Donald J.C., Goitein M., I-Chang M., Schneider R.J. and Wagner M., Rad. Res. 79 (1979) 34

Wainson A.A., Lomanov M.F., Shmakova N.L., Blokhin S.L. and Jarmonenko S.P., Brit. J. Radiol. 45 (1972) 525

Wilson R.R., Radiology 47 (1946) 487

Winzel E., Van Der Merwe E.J., Groenewald W., Pistorius S., Slabbert J.P., Robinson L. and Bohm L., S. Afr. Med. J. 71 (1987) 693